Assimilation of sea surface salinities from SMOS in an Arctic coupled ocean and sea ice reanalysis

Jiping Xie[1], Roshin P. Raj[1], Laurent Bertino[1], Justino Martínez[2], Carolina Gabarró[2,3], and Rafael Catany[4]

[1] Nansen Environmental and Remote Sensing Center and Bjerknes Centre for Climate Research, Bergen, Norway

[2] Institute of Marine Sciences, ICM-CSIC, Barcelona, Spain

[3] Barcelona Expert Center, Barcelona, Spain

[4] ARGANS, Plymouth, UK

Corresponding author: Jiping Xie, jiping.xie@nersc.no

1 **Abstract**

2 In the Arctic, the sea surface salinity (SSS) plays a key role in processes related to

3 water mixing and sea ice. However, the lack of salinity observations causes large

4 uncertainties in Arctic Ocean forecasts and reanalysis. Recently the Soil Moisture and Ocean

5 Salinity (SMOS) satellite mission was used by the Barcelona Expert Centre to develop an

6 Arctic SSS product. In this study, we evaluate the impact of assimilating this data in a

7 coupled ocean-ice data assimilation system. Using the Deterministic Ensemble Kalman filter

8 from July to December 2016, two assimilation runs respectively assimilated two successive

9 versions of the SMOS SSS product, on top of a pre-existing reanalysis run. The runs were

10 validated against independent in-situ salinity profiles in the Arctic. The results show that the

11 biases and the Root Mean Squared Differences (RMSD) of SSS are reduced by 10% to 50%

12 depending on areas, and highlight the importance of assimilating satellite salinity data. The

13 time series of Freshwater Content (FWC) further shows that its seasonal cycle can be

14 adjusted by assimilation of the SSS products, which is encouraging for its use in a long-time

15 reanalysis to better reproduce the Arctic water cycle.

16

17 **Keywords**: Arctic Ocean; Sea Surface Salinity; FWC; SMOS;

1. Introduction

The Arctic Ocean is undergoing a dramatic warming, resulting in the loss of sea ice documented by previous studies (Johannessen et al., 1999; Stroeve and Notz, 2018). Sea ice melt contributes freshwater to the Arctic Ocean, together with other sources, and has far-reaching effects on the Arctic Ocean environment (Carmack et al., 2016). The Arctic observing system, compared to other oceans, lacks the capability to provide a complete picture of ocean salinity, particularly because of obstruction by sea ice. A complete reconstruction of Arctic environmental variables thus requires a data assimilative numerical model capable of propagating information below sea ice during the winter as practiced by ocean operational forecast systems (Dombrowsky, 2009; Fujii et al., 2019). As with other ocean data assimilation (DA) applications, Arctic reanalysis products of ocean and sea ice play an important role in understanding climate change and its mechanisms. In recent years, many studies (Storto et al., 2019; Uotila et al., 2019) evaluated the quality of the Arctic reanalysis products and recommended experiments to maximize the usefulness of new observations, as done in Kaminski et al. (2015) and Xie et al. (2018). However, there are no impact studies of salinity observations in the Arctic to our knowledge.

Ocean salinity has been used to study the water cycle for the last 20 years (e.g., Curry et al., 2003; Boyer et al., 2005; Yu, 2011; Yu et al., 2017). A recent review paper showed a stabilization of the Freshwater Content (FWC) in the Arctic Basin, although observations indicate that the Beaufort Gyre keeps getting fresher (Solomon et al., 2021). Salinity variations have far-reaching implications for ocean mixing, water mass formation, and ocean general circulation, but suffer from large uncertainties in the Arctic, mainly due to sparse observations and the lack of a steady-state reference time period (e.g., Stroh et al., 2015; Xie et al., 2019). Measuring sea surface salinity (SSS) from passive microwave remote sensing is a comparatively new but promising way to reduce the uncertainty in salinity. Launched in November 2009, the Microwave Imaging Radiometer using Aperture Synthesis (MIRAS) instrument of the European Space Agency's (ESA) Soil Moisture and Ocean Salinity (SMOS) mission measures the brightness temperature (T_B) on the sea surface. The passive 2-D interferometric radiometer on the satellite operating in L-band (1.4 GHz) is sensitive to water salinity and sufficiently free from electromagnetic interference (e.g., Font et al., 2010; Kerr et al., 2010). Since May 2010, SMOS operationally provides SSS records over the global ocean (Mecklenburg et al., 2012). During the last 12 years, large improvements have been introduced in the SMOS data processing chain, increasing the accuracy and coverage of the salinity data up to levels that were unthinkable at the beginning of the mission (Martin-Neira et al. 2016, Olmedo et al., 2018; Reul et al., 2020; Boutin et al., 2022).

53   Furthermore, the assimilation of satellite-derived SSS products using an ensemble DA

54   method has been found to significantly improve the surface and subsurface salinity fields in

55   the tropics (Lu et al. 2016). The advantages of assimilating three SSS products from SMOS,

56   Aquarius (ref., Lee et al, 2012), and Soil Moisture Active Passive Mission (SMAP; e.g., Tang

57   et al., 2017) into a global ocean forecast system using 3D-Var DA method have also been

58   demonstrated by Martin et al (2019). Their results show the benefits of assimilating both the

59   SMOS and SMAP datasets in the intertropical convergence zone in the tropical Pacific.

60   However, very few studies investigated the impact of assimilating SSS products in the Arctic

61   or high latitudes. Since the beginning, the salinity retrieval from SMOS in cold regions has

62   been very challenging for three main reasons: i) the lower sensitivity of T_B in cold waters

63   leading to larger SSS error (Yueh et al., 2001; e.g, the sensitivity drops from 0.5 to 0.3 K

64   PSU^{-1} when sea surface temperature decreases from 15 to 5°C); ii) Land-sea and ice-sea

65   contaminations resulting from abrupt changes of T_B values across these two interfaces,

66   combined with the large ground footprint of SMOS; iii) the requirement of a well-observed

67   steady-state period for the removal of biases. Addressing these challenges in the SMOS

68   salinity retrieval approach, Olmedo et al. (2017) introduced a non-Bayesian retrieval method

69   to debias the Level 1 baseline (L1B) salinity against the reference SSS from Argo data. Level

70   1 data from the satellite is available within 24 hours, but the additional processing steps

71   require high-quality auxiliary data so that the Level 3 and 4 SSS are only provided in delayed

72   mode. Starting with the ESA L1B (v620) product from SMOS, the Barcelona Expert Centre

73   (BEC) released Version 2.0 of the Arctic gridded SSS product (25 km resolution; Olmedo et

74   al., 2018). Xie et al. (2019) evaluated the V2.0 SSS product and another gridded Arctic

75   SMOS SSS product developed by LOCEAN (Boutin et al., 2018) during the years 2011-

76   2013. These two SSS observations, together with an Arctic reanalysis (Xie et al., 2017) and

77   one objective analysis product (its upgradated product is available to see Greiner et al.,

78   2021), were validated against in-situ observations and compared with two climatology

79   datasets: the World Ocean Atlas of 2013 (WOA2013; *ref.*, Zweng et al., 2013) and the Polar

80   science center Hydrographic Climatology (PHC 3.0; *ref.*, Steele et al., 2001). They found

81   considerable discrepancies among the different gridded SSS products, especially in the

82   freshest seawater (<24 psu). The intercomparison of these Arctic SSS products shows room

83   for improvement of the SMOS-based SSS in the Arctic.

84

85   Recently, under the framework of the ESA project Arctic+Salinity (AO/1-9158/18/I-BG), and

86   further development of the non-Bayesian scheme (Olmedo et al., 2017), the effective

87   resolutions of SSS data were enhanced both in space and time (Martínez et al., 2022). The

88   new version of the SSS product (V3.1) shows the capability to monitor the mesoscale

89   structures and river discharges (e.g., Martínez et al., 2022). This new product provides daily

90   maps (Level 4) of 9-day averages in the Arctic on a regular 25 km grid and covers a longer

91   time period 2011-2019, and are released through the BEC portal (http://bec.icm.csic.es/ and

92   also at DOI: 10.20350/digitalCSIC/12620; last accessed May 2022). The major differences in

93   the estimation of the two SSS products (V2.0 and V3.1) are detailed in the Algorithm

94   Theoretical Baseline Document (ATBD) of the Arctic+Salinity project (Martínez et al., 2020).

95   Figure 1 shows that in comparison to V2.0, V3.1 provides wider coverage in the marginal

96   seas around the Arctic and is also fresher as indicated by the 26 psu isoline.

97   The two successive versions of the BEC SMOS SSS products are assimilated into the

98   TOPAZ Arctic reanalysis system (detailed in Section 2) during the summer of 2016. These

99   two assimilation runs are compared to the Arctic reanalysis without assimilation of satellite

100   SSS data which is identical to the product ARCTIC_REANALYSIS_PHYS_002_003 in the

101   Copernicus Marine Services. The model validation against independent observations

102   presents the differences stemming from these two SSS products, although they are from the

103   same initial data source (SMOS). Their impact on the assimilation in the Arctic coupled ice-

104   ocean model shows large differences, thereby motivating further efforts to improve SSS

105   retrievals in the cold Arctic.

106   The paper is organized as follows: Section 2 describes briefly the coupled ocean and sea ice

107   data assimilation system and the assimilation experiments; Section 3 describes the in-situ

108   observations and the validation metrics; results presented in Section 4 include the validation

109   using independent SSS observations, separated into different ocean basins. Section 4 also

110   examines the impact of SSS assimilation on the weekly increments of other related variables

111   near the surface, and explores the integrated effect on the freshwater simulated by the

112   model. In Section 5, the findings of this study and future perspectives are summarized.

113

114   **2.   Assimilation system and experimental design**

115   *2.1 The Arctic ocean and sea-ice coupled data assimilation system*

116   TOPAZ is a coupled ocean and sea ice data assimilation system, built using the

117   Deterministic Ensemble Kalman Filter (DEnKF; Sakov et al., 2012) to simultaneously

118   assimilate multiple types of observations for the ocean and sea ice (Xie et al., 2017). The

119   ocean model in this system uses version 2.2 of the Hybrid Coordinate Ocean Model

120   (HYCOM; Chassignet et al., 2003) with a low-distortion square grid with a horizontal

121   resolution of 12-16 km. The river discharge input is climatological, using the ERA-Interim

122   runoffs channeled in a simple hydrological model, which tends to underestimate the

123 amplitude of the seasonal cycle and thus a saline bias at the surface (Xie et al. 2019). The

124 coupled sea ice model uses a single-category thermodynamic model (Drange and Simonsen,

125 1996) and dynamics by the modified elastic-viscous-plastic rheology (Bouillon et al., 2013) in

126 an early version of the CICE model (Lisæter et al. 2003). The model covers the whole Arctic

127 Ocean (shown in Fig. 1 in Xie et al., 2017). A seasonal inflow of Pacific Water is imposed

128 across the Bering Strait, based on observed transports (Woodgate et al., 2012). At all lateral

129 boundaries, the temperature and salinity stratifications are relaxed to a climatology

130 combining version 2.0 of WAO2013 and version 3.0 of PHC with a 20-grid cells buffer zone.

131 To avoid a potential model drift, the surface salinity is relaxed to the combined climatology as

132 mentioned above, with a 30-day timescale, but the relaxation is suppressed wherever the

133 difference from climatology exceeds 0.5 psu to avoid the artificial formation of stable surface

134 freshwater layers.

135 The two steps of the assimilation system can be translated by the following concept

136 expressions (update and model propagation):

$$X_a = X_f + K(y - HX_f) \tag{1}$$

$$X_f = M(X_a) \tag{2}$$

139 Where the matrix **X** represents the model states with all 3-D and 2-D variables needed by

140 the model forward integration, represented by the operator M. The subscripts 'a' and 'f'

141 respectively indicate the analyzed model state obtained through optimization after DA and

142 the model forecast. The vector **y** is composed of the quality-checked observations during the

143 weekly cycle, the observation operator H gives the model equivalent matching the

144 observations. The innovation term (in parentheses in Eq.1) represents the differences

145 between the model and the various observations on the observation space. The TOPAZ

146 model runs an ensemble of 100 members. The **K** matrix (Kalman gain) is calculated using

147 the ensemble covariance matrix. On a weekly basis, we use the DEnKF to assimilate

148 different types of ocean and ice observations, including along-track sea level anomaly (SLA),

149 sea surface temperature (SST), in-situ profiles of temperature and salinity, sea ice

150 concentrations (SIC) and sea ice drift products all sourced from the Copernicus Marine

151 Environment Monitoring Services (CMEMS; https://marine.copernicus.eu). The same TOPAZ

152 system provides a 10-day forecast of ocean physics and biogeochemistry in the Arctic

153 (Bertino et al., 2021) every day via the CMEMS portal. Like other square root versions of the

154 Ensemble Kalman Filter, the DEnKF splits Eq. 1 into two steps: the K calculation is applied to

155 the ensemble mean, and the anomalies are updated to match a target analysis covariance

156 (more details in Sakov et al., 2012).

157

2.2 Assimilation experiments and the observation error estimate for SSS

159   To evaluate the impact of the assimilation of two versions of the SSS products on TOPAZ

160   model runs, a control assimilation experiment (Exp0) and two parallel assimilation

161   experiments (ExpV2, ExpV3) for a 6-month time period (July to December 2016) were

162   performed. Exp0 assimilates all available ocean and sea ice data, except the satellite SSS

163   product. On the other hand, ExpV2 and ExpV3 additionally assimilate the BEC SSS products

164   V2.0 and V3.1, respectively. Details of the three assimilation runs are listed in Table 1.

165   The observation error is a key parameter in any DA system: Too small values lead to

166   overfitting, while too large values make the assimilation inefficient. The salinity errors from

167   Passive Microwaves were previously estimated by Vinogradova et al. (2014): the zonal

168   average of standard errors north of 60°N was estimated at 0.6 psu. In a recent study, Xie et

169   al. (2019) evaluated the SMOS-based SSS products using in-situ observations and revealed

170   strong regional dependence for the V2.0 product errors: smaller than 0.4 psu in the Northern

171   Atlantic but increasing dramatically to 1 psu in the Nordic seas and over 2 psu in the central

172   Arctic. Undoubtedly, the salinity observation errors from Passive Microwaves are higher in

173   high latitudes than elsewhere. Furthermore, in the Beaufort Sea (as Fig. 12a in Xie et al.,

174   2019), the error of the SSS V2.0 product and the Arctic reanalysis product from TOPAZ

175   (same as Exp0 used in this study) both show an inverse relationship between SSS values

176   and SSS errors. Hence, we use an empirical error function for ExpV2 and ExpV3 adjusted to

177   the discrepancies as shown in Eq. 3, following Xie et al. (2019):

178    $$E_{SSS} = max\left\{E_{int}, [0.6 + \frac{6}{1+exp\left(\frac{SSS-16}{5}\right)}]^2\right\} \qquad (3)$$

179   Where E_{int} is the instrumental error variance estimated by the data provider, that part is

180   absent from the V2.0 product. Eq. 3 yields more conservative error estimates than the

181   providers, which also prevents the discontinuities caused by strong assimilation updates (as

182   an example noticed by Balibrea-Iniesta et al., 2018). Other precautions are also applied

183   following Sakov et al. (2012). By construction, the observation errors are always larger for

184   the V3.1 than the V2.0 product, but in fresh waters they are identical. This implies that the

185   assimilation may pull the analysis closer to the V2.0 than the V3.1 product in the more saline

186   waters, but they are otherwise treated on equal footing, ignoring the a priori expectation that

187   the most recent product should be more reliable.

188

189   **3.   In-situ SSS observations for validation**

190   All in-situ salinity profiles were collected from various repositories and cruises (as shown in

191   Fig. 2). Salinity measurements were extracted near the surface over the Arctic domain during

192   the experimental time period. The sanity check procedures include: i) location check to

193 ensure observation in the water grid same as the model used; ii) omit the invalid profiles if
194 the top depth is deeper than 8 m; iii) remove redundant observations. Since the model does
195 not reproduce local gradients of the vertical salinity profiles shown in Supply et al. (2020), all
196 the salinity profiles are averaged over the upper 8 meters below the surface. This also avoids
197 the loss of the profiles that do not reach the surface.

198 ● *Data from the Beaufort Gyre Experiment Project (BGEP)*
199 The BGEP has maintained an observing system in the Canadian Basin since 2003 and
200 provides in-situ observations over the Beaufort Gyre every summer. Although the BGEP has
201 maintained three bottom-tethered moorings since 2003, the shallowest depth of the
202 measured profiles for temperature and salinity is below 50 m. Hence, in this study, we only
203 use the Conductivity Temperature Depth (CTD) dataset from the cruise in 2016
204 (https://www2.whoi.edu/site/beaufortgyre/data/ctd-and-geochemistry/, last access: 14th
205 February 2022). SSS observations from these CTD profiles in the time period from 13th Sep
206 to 10th Oct 2016 are represented by the red triangles in Fig. 2.

207 ● *Data from Oceans Melting Greenland (OMG)*
208 The project Oceans Melting Greenland was funded by NASA to understand the role of the
209 ocean in melting Greenland's glaciers. Over a five-year campaign, this project collected
210 temperature and salinity profiles by Airborne eXpendable Conductivity Temperature Depth
211 (AXCTD) launched from an aircraft (*e.g.*, Fenty, et al, 2016). The deployed probe can sink to
212 a depth of 1000 meters, connected with a float by a wire. The measured temperature and
213 conductivity are then sent back to the aircraft. These salinity profiles collected during the first
214 OMG campaign in 2016 are downloaded from
215 https://podaac.jpl.nasa.gov/dataset/OMG_L2_AXCTD/ (last access: 10th February 2022). The
216 SSS from OMG distributed around Greenland, from 13th Sep to 10th Oct 2016 are shown as
217 the inverted blue triangles in Fig. 2.

218 ● *Data from the International Council for the Exploration of the Sea (ICES)*
219 Salinity profiles were also obtained from the ICES portal (https://www.ices.dk). Shown as
220 blue squares in Fig. 2, the locations of the profiles during the last 6 months of 2016 are
221 dense in the Nordic Seas and restricted to north of 58°N for this study. Valid salinity profiles
222 from ICES (last access: 9th February 2022) are obtained from 6th July to 23rd Nov in 2016.

223 ● *Data from other cruises at the Arctic Data Center (ADC)*
224 Surface salinity observations from scientific cruises are obtained from the Arctic Data
225 Center portal (https://arcticdata.io/catalog/data; last access: 17th Feb 2022). During the
226 model experiment, the first relevant cruise in ADC was SKQ201612S which was operated by
227 University of Alaska Fairbanks with the RV Sikuliaq. This cruise collected data from Nome,

228   Alaska on 3rd September, to the northeast Chukchi Sea, and then back to Nome at the end of

229   September 2016. The temperature and salinity profiles were collected by a Sea-Bird 911

230   CTD instrument package. All measurements at each station were done both down- and up-

231   cast ways. To produce water column profiles at each station, the down-cast data were

232   binned at 1 m intervals (Goñi et al.,2021). Besides the CTD profiles of SKQ201612S, more

233   seawater samples were collected via the surface underway system on the RV Sikuliaq.

234   Through a sea chest below the waterline (e.g., 4-8 m), the uncontaminated seawater was

235   pumped into the ship and the corresponding filtration system supplies samples every 3 hours

236   to the sensors (More details in Goñi et al., 2019). These SSS observations were obtained on

237   the 9th-27th of September, indicated as blue crosses in Fig. 2.

238   Moreover, SSS measurements were also collected from the Seabird CTD on board Sir

239   Wilfrid Laurier (SWL), but only in July 2016. This cruise is part of the annual monitoring from

240   the Canadian Coast Guard Service (Cooper et al., 2019). The SSS observations are

241   obtained near the Bering Strait close to the Pacific boundary of our model.

242   After skipping the diurnal signals in observed surface salinity, all valid SSS measurements

243   from the above data sources are compared with the daily average SSS of the three

244   assimilation experiments listed in Table 1. All the assimilation runs use a weekly assimilation

245   cycle: The model runs forward 7 days after each assimilation step and provides daily

246   averages for each day from the ensemble mean, which we refer to as "forecast" even when

247   using delayed-mode observations and atmospheric forcings. The model data has been

248   collocated with the observations for validation. To estimate the forecast differences to

249   observations, we use the standard statistical moments:

250
$$Bias = \sum_{i=1}^{N} \sum_{1}^{O_i}(H\bar{X}_i - y_i) \ / \sum_{i=1}^{N} O_i \tag{4},$$

251
$$RMSD = \sqrt{\sum_{i=1}^{N} \sum_{1}^{O_i}(H\bar{X}_i - y_i)^2 \ / \sum_{i=1}^{N} O_i} \tag{5},$$

252   Where i is the ith day, O_i represents the number of observations on this day, and N

253   represents the total number of days depending on the source of observations. Then $\bar{X}_i$

254   represents the model daily average at the observation time as the ensemble means of 100

255   model members. H is an operator to extract the SSS simulation from the model at the

256   observed location. The model performance can then be quantitatively compared between the

257   three assimilation runs.

258   In addition, we further introduce a two-sample Student's t-test to evaluate the significance of

259   the change of SSS bias in ExpV2/ExpV3 with respect to Exp0. Compared to in-situ

260   observations, the SSS misfits in Exp0 are the error array **e$_1$**. The corresponding error array

8

261   from ExpV2 or ExpV3 is called $\mathbf{e_2}$. Thus, considering the null hypothesis H0: $\bar{e}_1$ and $\bar{e}_2$ are

262   the means of indiscernible random draws, the t-value can be calculated as follows:

263
$$t = \frac{|\bar{e}_2 - \bar{e}_1|}{\sqrt{s_1^2/(n_1 - 1) + s_2^2/(n_2 - 1)}}$$

264   Where $s_1(s_2)$ is the standard deviation in the $\mathbf{e_1}(\mathbf{e_2})$, and n_1 (n_2) is the number of observations.

265   For every t-value, the p-value from the above equation is the probability that random errors

266   would prove H0 wrong. Low p-values (<0.05) indicate that the change of bias due to

267   assimilation is significant.

268
269   **4. Results**

270   *4.1 Diagnosing using assimilation statistics*

271   The SSS innovations in the two assimilation runs ExpV2 and ExpV3 are compared in Fig. 3,

272   together with the number of assimilated SSS observations and the ensemble spread

273   calculated by the ensemble standard deviation. The total number of observations is at its

274   maximum in September when the sea ice cover is minimal. Since both versions of the SSS

275   product share the same time-frequency (9-day average) and gridded format, the number of

276   assimilated observations in the two runs remains identical (gray lines in Fig. 3). For ExpV2,

277   the Root Mean Square (RMS) of the SSS innovation varies between 0.4 and 1.2 psu, but the

278   mean of SSS innovation, calculated as the observation minus the model simulation (cf. the

279   bracket in Eq.1), shows the saline bias of 0.4 psu, highest in September. However, in ExpV3

280   the salinity bias quickly disappears after a few data assimilation cycles. The RMS of the SSS

281   innovation is larger in ExpV3 between 0.6 and 1.6 psu, which can partly be explained by the

282   higher effective resolution of the V3.1 product and the double penalty effect. In ExpV3, the

283   RMS of the SSS innovation (the red line) jumps down after the first SSS assimilation step.

284   The RMS of SSS innovations and the observation errors both decrease from summer to

285   winter, following a seasonal cycle as the areas of fresher water get gradually ice-covered.

286   The domain-averaged observation errors are only slightly larger in ExpV3 than in ExpV2, as

287   explained above, and the RMS of SSS innovations become lower than the observation errors

288   near the end of the run, which indicates that the observation errors for the V2.0 SSS have

289   been overestimated.

290   In the top panels of Fig. 4, the SSS maps present the control run (Exp0) in August and

291   September 2016, respectively. For Exp0 in August, low salinity waters are found in the

292   Beaufort Sea near the Mackenzie River and along the East Siberian coast. In September, the

293   fresher waters, below 30 psu, bridge the two areas in Exp0 probably due to sea ice melt,

294   although the lowest salinity near the Siberian coast remains unchanged from August to

295   September (as indicated by the 28 psu isoline). Compared with the SSS observations from

296   SMOS (Fig. 1), these two low salinity waters are clearly underestimated in Exp0. Meanwhile,

297   the relatively saline 32 psu isoline crosses both the Eurasian basin and the Baffin Bay. In the

298   Laptev Sea, due to the significant effects of river runoff and ice melt, the salinity shows a

299   strong gradient from the southeast to the northern part. During winter, the salinity increases

300   to 34 psu, and decreases in summer near to 30 psu (Janout et al., 2017). In the northwest

301   Laptev Sea, the saline tongue of 32 psu extends eastward to Taymyr Peninsula (TP). North

302   of the TP, the Kara Sea freshwater meets with the Atlantic Water pathways from the Fram

303   Strait and Barents Sea (shown in Figure 1 by Janout et al., 2017). Close to the TP, the

304   observations at the mooring profiles in Janout et al. (2017) show much fresher surface

305   salinity (29 psu) than the subsurface salinity (32 psu) in summer. Compared to the SMOS

306   SSS maps (Fig. 1), only the V3.1 product shows the 32 psu isolines around the TP. Another

307   difference between the two SMOS products arises in the Chukchi Sea where the V3.1

308   product is more saline than both the V2.0 product and SSS in Exp0.

309   Then the middle and bottom panels of Fig. 4 show the SSS differences in August and

310   September 2016 between the SSS assimilation runs and the control run. Fig. 4c and 4d both

311   show a freshening of the coastal areas in the Kara Sea, Laptev Sea, and East Siberian Sea,

312   but in ExpV3 the freshening is stronger and wider (Fig. 4e and 4f). In the Beaufort Sea,

313   ExpV2 mainly brings a local freshening near the mouth of the Mackenzie River in August,

314   which then spreads out along the coast in September. The freshening in the BS brought by

315   ExpV3 affects a broader area, even including the Canadian Archipelago. ExpV3 also

316   freshens the SSS on both sides of Greenland Island. From August onwards, the SSS in

317   ExpV3 freshens by over 1 psu along the whole east Greenland coast, which clearly does not

318   happen in ExpV2. In fact, the 32 psu isoline in ExpV3 (not shown) extends hundreds of

319   kilometers further to the South East Greenland coast in comparison to Exp0 and ExpV2. The

320   rest of the Greenland coast is also fresher by 0.5 psu in ExpV3 during both months. This is a

321   sign of a consistent change in the V3.1 product.

322   Even though most of the SSS assimilation leads to a freshening of the surface, a few

323   locations show higher salinity than Exp0, these are different from ExpV2 to ExpV3. For

324   example, the saline increment near the Bering Strait is larger in ExpV3 in excess of 1 psu,

325   consistently with the difference between the two remote sensing products (Fig. 1).

326   Other increases in SSS concern small areas near estuaries and are more common in ExpV3.

327   The increase to the west of the Yamal Peninsula can be explained by a model setup bias in

328   the location of the Ob river but compensated by the SSS assimilation. In the above

329   comparisons of SSS maps, the central Arctic is not discussed, since the region is covered by

330   sea ice and the effect of assimilation is indirect.

331

4.2 Comparison with independent in-situ observations

333   Quality-checked in-situ observations in the Central Arctic are very unevenly distributed. After

334   pooling all platforms together, we further investigate the SSS misfits in six subregions of the

335   Arctic (Fig. 2 and Table 2). This section will present statistics of differences to independent

336   in-situ observations, separately considering marginal seas.

337

338   *Beaufort Sea (BS):* Figure 5 shows the scatterplots of SSS in the three runs against in-situ

339   observations from BGEP, OMG, and ICES. In the Beaufort Sea (top panel in Fig. 5), the

340   observed SSS varies in a range of 26-29 psu. The range of SSS in Exp0 is much smaller,

341   between 29-31 psu with a saline bias of 2.6 psu and an RMSD of 2.7 psu, but otherwise, it

342   shows a reasonably linear relationship (r=0.59). The SSS bias in Exp0 has the same value

343   as in Xie et al. (2019), although estimated using the BGEP observations in a different time

344   period (2011-2013). The range of SSS in ExpV2 is slightly improved to 28-30.5 psu. Further,

345   the bias is reduced by 0.5 psu, corresponding to bias and RMSD reductions of respectively

346   13.5% and 10.5% with respect to Exp0. In ExpV3, the SSS range is much closer, between

347   26.5 and 30.5 psu, and the resulting bias and RMSD reductions of SSS are respectively

348   26.3% and 17.3% with respect to Exp0. Both the bias reduction in ExpV2 and ExpV3 relative

349   to Exp0 pass the significance test ($\alpha = 0.05$) through Student's t-test. Furthermore,

350   compared to all in-situ SSS in BS (top panels in Fig. 7), the SSS misfits in ExpV3 show a

351   stronger reduction by 26.0% for bias and 20.6% for RMSD. ExpV2 reduces these errors by

352   half as much (13.5% for bias and 11.5% for RMSD). These results clearly indicate that the

353   new version of the SSS is more beneficial for data assimilation in the Beaufort Sea.

354

355   *Chukchi Sea (CS)*: Fig. 6 shows the SSS deviations as a function of time during the SKQ

356   cruise route. Figure 6a shows the surface levels from CTDs. The saline bias (2.8 psu) is

357   more pronounced than in the Beaufort Sea, which we attribute to the proximity to the model

358   boundary in the Bering Strait, relaxed to climatological values, where the interannual

359   variability of Pacific water is not included. After assimilating SSS products, a reduction of the

360   bias is observed during September, by 15.5% in ExpV2 and up to 22.2% in ExpV3. The

361   comparison to underway surface water samples (Fig. 6b) also shows an error reduction of

362   around 15%, though fewer differences between ExpV2 and ExpV3.

363   Considering other cruise data in the CS (Fig. 7; bottom panels), the SSS in Exp0 shows

364   almost uniform values with a saline bias of about 2.3 psu and an RMSD of 2.6 psu. A recent

365   observational study by Goñi et al. (2021) shows that the surface salinity of the CS during late

366   summer varies between 28-30 psu during the time period 2016-2017. The range of SSS

367   observations considered here is slightly broader (27-32 psu). The assimilation of SSS

368   products reduces the misfits (bias and RMSD). As in the BS, the SSS in ExpV3 has more

369   significant reductions in bias (17.7%) and RMSD (16.4%). After assimilation, the deviations

370   are in the same range as found in the BS. All the bias reductions in ExpV2 and ExpV3 are

371   significant compared to Exp0 through the t-test ($\alpha = 0.05$).

372

373   *Greenland Sea (GS)*: Most SSS observations around Greenland are from the OMG

374   programme, shown as the blue downward triangles in Fig. 2. Considering first all SSS

375   observations from OMG, the SSS misfits in the three runs (shown in the middle panels of Fig.

376   5) show smaller bias and RMSD than in the BS and the CS. However, the SSS in ExpV3 still

377   brings significant error reductions with a reduction of 32.6%/9.4% of the bias and RMSD

378   compared to Exp0. Notably, the SSS misfits in ExpV2 are almost identical to Exp0, which

379   indicates that the V2.0 SSS product was not informative there.

380   We now separate the evaluation in the East and West of Greenland covering the GS and

381   Baffin Bay (BB) areas as shown in Fig. 2 (also listed in Table 2). The top panel of Fig. 8

382   shows that all SSS observations available in the GS vary between 27 and 35 psu. This large

383   range includes fresh coastal waters, Arctic water, and Atlantic Water. The three assimilation

384   runs show different saline biases, especially for salinities lower than 30 psu. While in

385   observations the minimum salinity is below 28 psu, it only reaches 30 psu in ExpV3, and 31

386   psu in both Exp0 and ExpV2. As a result, the bias reduction in ExpV3 is over 50% and the

387   RMSD decreased by about 10.5% in the GS. ExpV2 is disappointingly similar to Exp0. This

388   is also the case in BB (shown in Fig. 8 bottom row), where differences between ExpV2 and

389   Exp0 are less than 0.02 psu. In contrast, ExpV3 reduces the SSS bias but does not

390   significantly reduce the RMSD in the BB. One possible explanation is the double-penalty

391   effect because the V3.1 product has a higher effective resolution than V2.0. This can be

392   seen in Fig. 8 as the ExpV3 values are more scattered.

393   Finally, we examine the SSS deviations in the Barents Sea and the Norwegian Sea. The

394   SSS bias and RMSD are the lowest in ExpV3 in Table 2, even though the reductions are not

395   as significant as in the area of fresher surface waters. Compared to the ICES observations

396   distributed in the North Atlantic and the Nordic Seas (blue squares in Fig. 2), the scatterplots

397   of Exp0 and ExpV2 are nearly identical (see the bottom panels in Fig. 5). The minimum

398   salinity in these two runs is 32 psu. The SSS bias and RMSD in both runs are also similar

399   (differences less than 0.01 psu). In contrast, lower salinity values are found in ExpV3, below

400   32 psu, although the saline bias remains around 0.5 psu on average. Notably, the SSS in

401   ExpV3 shows that data assimilation can reduce the bias by 15% compared to Exp0, but the

402   RMSD only reduced about 0.03 psu, also possibly due to the double penalty effect. This also

403   suggests that the improvements near the coast will be the next challenge for future versions
404   of the SSS product.
405
406   *4.3 Impact analysis of SSS assimilation*
407   The above section has demonstrated that the assimilation of remote sensing SSS generally
408   improves the match to independent in-situ measurements, although the improvements are
409   location-dependent. Since large areas are void of in-situ measurements, the increment
410   changes of other surface variables caused by assimilation from the three runs will also be
411   meaningful in understanding the impacts incurred. The increments are the differences
412   between the analysis and the forecast. The calculation of them is the result of the innovations
413   of all assimilated observations multiplied by the Kalman gain, as computed in Eq. (1). Since
414   the DEnKF update is multivariate, we present the impact of the assimilation on other model
415   variables closely related to the SSS: SST and SIC. Since the only difference in the setting
416   between the three runs is the assimilation of SSS, we can attribute the differences to the
417   impact of SSS observations. In theory, if both the model and observations were unbiased,
418   the increments of other assimilated variables should generally decrease because of the
419   presence of a new SSS term in the denominator of the Kalman Gain (the assimilated
420   observations compete with each other), but SSS biases can also spill over the other model
421   variables and increase the innovations on the following assimilation step and thus the
422   resulting increments. Hypothetically, if the SSS were the only source of errors in TOPAZ, the
423   increments of other variables should vanish over time. Figure 9 compares the time-averaged
424   increments of SIC and seawater temperature in the top 3-m layer (considered as SST here)
425   in the three runs. The sign of the increments remains overall the same across the three
426   experiments, both for SST and SIC. The SST increments in the three runs are negative in the
427   open ocean and positive near the ice edge, as shown in the right column of Fig. 9.
428   The SST increments in Exp0 and in ExpV2 are nearly identical, but in ExpV3 there are few
429   areas such as in the Kara Sea and in the Laptev Sea where the SST increments have been
430   suppressed. These are locations where the SSS and SST are positively correlated, so the
431   updated SSS by assimilation is also helpful in reducing the water temperature misfits near
432   the surface. The changes in SST are however small with respect to the large SSS
433   differences in Figure 4. In Exp0, the SIC increments are small (<5%) inside the ice pack. The
434   satellite SIC observations are assimilated every week and help to correctly position the ice
435   edge (Sakov et al., 2012). The increments exceed 5% along the ice edge, as can be seen in
436   the northern Barents Sea.
437   The assimilation of the V2.0 SSS product also shows minimal differences from Exp0 partly
438   because of the conservative sea ice mask in the V2.0 SMOS SSS. The SIC increments are

13

439 opposite to those of SST, showing that the assimilation warms the surface water where ice is

440 removed, which is consistent with Lisæter et al. (2003). Only minor differences between

441 ExpV2 and ExpV0 are visible along all areas swept by the ice edge during the 6-month

442 experiment, for example in the Kara Sea. In contrast, the assimilation of the V3.1 SSS

443 product shows larger changes of SIC increments than in ExpV2 with a broader area of

444 negative increments (removed ice) in the northern Barents Sea. This is not visibly related to

445 the SST increments but to the freshening caused by the assimilation of V3.1 SSS as SSS

446 and SIC are positively correlated in the northern Barents Sea, as shown by Fig. 2 in Sakov et

447 al. (2012). The increased SIC increments may be an indication that the SSS freshening could

448 be excessive.

449 Since the whole water column is updated by the assimilation, the freshwater content is also

450 modified by the assimilation of SSS. There are however complex relationships between SSS

451 and FWC as shown by Fournier et al. (2020). The changes in FWC in the Arctic are

452 calculated as in Eq. (6) derived from Proshutinsky et al. (2009), although this method was

453 initially intended for the BS. Applying the same formula for interpolation of in-situ

454 observations, Proshutinsky et al. (2020) estimated the time-averaged summer freshwater

455 content in the Beaufort Gyre region in two time periods (1950-1980 and 2013-2018). In the

456 latter period, they located the FWC centre in the BS around (150°W, 75°N) and drew the 20-

457 m isoline over more than 5 degrees of latitude and nearly 30 degrees of longitude on

458 average. When compared to the earlier reference period, the FWC in the BS has increased

459 and its centre has shifted westward.

460 Following Proshutinsky et al. (2009), the model FWC in the Arctic is estimated as:

461 $$FWC = \int_{z_0}^{z_{ref}} (1 - \frac{S_{(z)}}{S_{ref}}) dz \qquad (6)$$

462 Where the reference salinity value S_{ref} is taken at 34.8 psu, z_{ref} is the depth of the reference

463 salinity or the sea bed, and $S(z)$ is the salinity profile. Figure 10 shows the FWC on two

464 representative days, September 20th and October 20th, 2016. In Exp0, the reanalysis

465 reproduces the typical FWC distribution in the Arctic with a maximum in the Beaufort Sea.

466 The 20 m isolines in Fig. 10a and 10d show an increase in spatial coverage during October,

467 consistent with Rosenblum et al. (2021), but the 20 m isoline is not extending as far as 170°E

468 compared to Proshutinsky et al. (2020). After assimilation of SSS products (either V2.0 or

469 V3.1), the amplitude and the spatial distribution of the FWC maximum increase slightly in the

470 BS (see Fig. 10b and 10c). A much larger increase of FWC appears on the East Siberian

471 shelf and in the coastal areas of the Laptev Sea and eastern Kara Sea, although to a

472 different extent in ExpV2 and in ExpV3. In the eastern Kara Sea, the FWC increases over a

473 wider area in ExpV2 than in ExpV3. To the west of the Yamal Peninsula, ExpV3 shows a

474 negative anomaly related to an incorrect location of the model river runoff, corrected in later
475 versions of the model. The SSS assimilation is able to correct the related fresh bias. In the
476 central Arctic, although the assimilated SSS measurements are masked by the sea ice
477 cover, the FWC differences north of 84°N are more pronounced in October than in
478 September, which indicates the advection of SSS increments by the Transpolar Drift Stream
479 (Rigor et al., 2002; Balibrea-Iniesta et al., 2018). These results suggest that the SSS
480 assimilation of both versions of SMOS satellite products will compensate for the insufficient
481 river summer runoff, redistribute the freshwater in the Arctic, and adjust the freshwater
482 budget. However, because of the limited in-situ data, the above assessment remains
483 qualitative.
484 Further, we compare the daily time series of Arctic-averaged FWC from the three runs to the
485 north of 70°N (Fig. 11). The FWC increases in October-November to reach its maximum, and
486 gradually decreases thereafter. The impact of weekly data assimilation cycles is visible as
487 instantaneous jumps on the three curves of the time series, but the assimilation of SSS does
488 not cause unrealistic imbalances. The FWC increases substantially due to SSS assimilation,
489 by about 25 cm. Notably, the assimilation of version 3.1 SSS causes a faster increase during
490 the first two months. Due to the absence of ground truth data in 2016, the above comparison
491 remains qualitative, but the timing of the peak is in better agreement with the ITP data
492 presented by Rosenblum et al. (2021, their Fig. 4), although the amplitude of the seasonal
493 FWC seems too small in all experiments, which can be related to insufficient thick ice in
494 TOPAZ (Uotila et al., 2019). More concrete evidence about the changed FWC will be
495 provided when the longer assimilation of the satellite-based SSS product is finished in the
496 near future.

497

498 **5.   Summary and discussions.**
499 The gridded SSS products from the SMOS satellite undoubtedly provide a way to constrain
500 errors in salinity, especially for an ocean reanalysis system. The present study is the first
501 observing system simulation experiment for the assimilation of SMOS SSS in the Arctic. In
502 this study, based on the TOPAZ reanalysis system, we compared the reanalysis assimilating
503 conventional observations with and without the assimilation of two successive SMOS SSS
504 products from BEC.
505 After comparison with independent SSS observations from CTD and surface water samples
506 along the cruises, the near-surface salinity errors have been significantly reduced compared
507 to the control experiment (Exp0). In the Beaufort Sea, the SSS bias and RMSD in ExpV3 are
508 reduced respectively by 26.0% and 20.6%. In ExpV2, the RMSD reduction is smaller (by

15

509 11.5%). In the Chukchi Sea, the reduction in SSS misfits in ExpV3 (bias:17.7%; RMSD:

510 16.4%) is also larger than in ExpV2 (bias: 15.5%; RMSD: 13.7%). Around Greenland, the

511 difference between the two products is even more pronounced, with a significant reduction in

512 the SSS bias (32.6%) and RMSD (9.4%) in ExpV3, while there is no notable improvement in

513 ExpV2. The difference is larger in the East Greenland Sea. The direct assimilation of SSS

514 from SMOS is more efficient at constraining the near-surface salinity than the multivariate

515 impact of other observations. This finding is also consistent with other SSS assimilation

516 experiments in the tropics (Chakraborty et al., 2015; Tranchant et al., 2019). Conversely,

517 when considering the multivariate impact of SSS on SIC (in Fig. 9) we find that the

518 assimilation of the V2 product does not affect the assimilation of sea ice concentrations while

519 the V3.1 product causes an increase in the negative increments, which could be an

520 indication of excessive freshening along the Siberian coasts. In contrast, the increments of

521 SST in the open ocean are smaller in ExpV3, indicating a synergy effect of SST and SSS.

522 Overall, our data assimilation system did not detect obvious inconsistencies between the

523 SMOS SSS product and other assimilated observations.

524

525 Furthermore, this study shows error reductions of SSS when assimilating the V3.1 product

526 from SMOS even outside of the central Arctic in the Nordic Seas and along the Norwegian

527 coast. Moreover, our analysis shows how the spatial distribution of Arctic FWC changes as a

528 result of assimilating the two SMOS products. The time series of averaged FWC north of

529 70°N shows that the FWC in the whole central Arctic can be increased by about 25 cm using

530 DA. Our experiments show that the Arctic FWC can be redistributed horizontally after

531 assimilation, but the latter effect requires a longer assimilation run to be evaluated.

532 As a summary of the quantitative SSS comparisons (Table 2), the overall score of each

533 assimilation setup for each subregion can be defined by its ability to reduce the SSS bias

534 and RMSD by more than 9% relative to Exp0 (Fig. 2). If both bias and RMSD meet the

535 objective, we give a score of 1, but of 2 if only one of them is met. If neither of them exceeds

536 9%, the score is set to 3. Thus outside of the central Arctic, the v2.0 SSS product loses its

537 impact on the TOPAZ system, but the V3.1 SSS brings significant impacts across the Arctic

538 and further out, and clearly benefits from its refined effective resolution (Martínez et al.,

539 2022). Since there was little evidence of a double-penalty effect in the validation RMSD apart

540 from Baffin Bay, we consider that the assimilation of the higher resolution signals was

541 efficient. However, the assimilation did not improve the SSS significantly in the Barents Sea

542 or other areas where SSS gradients are weak. These may require higher accuracy to

543 distinguish the Atlantic waters from other water masses of salinity only slightly below 35 psu.

544 To further improve the SSS product, a combination with the Aquarius sensor using the same

545   L-band frequency (e.g., Lee et al, 2012), and SMAP (e.g., Tang et al., 2017; Reul et al.,

546   2020) is desirable.

547

548   **Data availability.** All the in-situ observations for validation in this study are open access as

549   indicated in Sect. 3. The model results from Exp0 are the released TOPAZ reanalysis, which

550   is freely available from CMEMS (http://marine.copernicus.eu) or

551   https://doi.org/10.11582/2022.00043. The other assimilation experiments can be provided

552   freely upon personal communication.

553

554   **Author contributions**. JX initiated the design and carried out the assimilation

555   experiments. LB and RR contributed to the result interpretation. JM provided the SSS data.

556   CG and RC contributed to the uncertainty of the satellite data. All the authors contributed to

557   editing and correcting this paper.

558

559   **Competing interests.** The authors declare that they have no conflict of interest.

560

573

574   **Reference:**

575 Balibrea-Iniesta, F., Xie, J., Garcia-Garrido, V., Bertino, L., Maria Mancho, A., and Wiggins,
576   S.: Lagrangian transport across the upper Arctic waters in the Canadian Basin. Q. J. Roy.
577   Meteor. Soc., 145(718), 76-91, doi:10.1002/qj.3404, 2018.

578 Bertino, L., Ali, A., Carrasco, A., Lien, V., and Melsom, A.: THE ARCTIC MARINE FORECAST-
579   ING CENTER IN THE FIRST COPERNICUS PERIOD. 9th EuroGOOS International
580   conference, Shom; Ifremer; EuroGOOS AISBL, May 2021, Brest, France. pp.256-263. hal-
581   03334274v2. (Available from https://hal.archives-ouvertes.fr/hal-03334274v2/document)

582 Bouillon, S., Fichefet, T., Legat, V., and Madec, G.: The elastic-viscous-plastic method revised,
583   Ocean Modell., 7, 2–12, doi:10.1016/j.ocemod.2013.05.013, 2013.

584 Boutin, J., Jean-Luc, V., and Dmitry, K.: SMOS SSS L3 maps generated by CATDS CEC
585   LOCEAN, debias V3.0. SEANOE. 2018. Available online:
586   https://www.seanoe.org/data/00417/52804/.

587 Boutin J., Vergely J.-L., and Khvorostyanov D.: SMOS SSS L3 maps generated by CATDS
588   CEC LOCEAN. debias V7.0. SEANOE. doi:10.17882/52804#91742, 2022.

589 Boyer, T. P., Levitus, S., Antonov, J. I., Locarnini, R. A., and Garcia, H. E.: Linear trends in
590   salinity for the World Ocean, 1955–1998, *Geophys. Res. Lett.*, 32, L01604,
591   doi:10.1029/2004GL021791, 2005.

592 Carmack, E. C., Yamamoto Kawai, M., Haine, T. W. N., Bacon, S., Bluhm, B. A., Lique, C.,
593   Melling, H., Polyakov, I. V., Stra- neo, F., Timmermans, M.-L., and Williams, W. J.:
594   Freshwater and its role in the Arctic Marine System: Sources, disposition, storage, export,
595   and physical and biogeochemical consequences in the Arctic and global oceans, J.
596   Geophys. Res. Biogeo., 121, 675–717, doi:10.1002/2015JG003140, 2016.

597 Chakraborty, A., Sharma, R., Kumar, R., and Basu, S.: Joint Assimilation of Aquarius-derived
598   Sea Surface Salinity and AVHRR-derived Sea Surface Temperature in an Ocean General
599   Circulation Model Using SEEK Filter: Implication for Mixed Layer Depth and Barrier Layer
600   Thickness, J. Geophys. Res. Oceans, 120 (10), 6927-6942, doi:10.1002/2015JC010934,
601   2015.

602 Chassignet, E. P., Smith, L. T., and Halliwell, G. R.: North Atlantic Simulations with the Hybrid
603   Coordinate Ocean Model (HYCOM): Impact of the vertical coordinate choice, reference
604   pressure, and thermobaricity, J. Phys. Oceanogr., 33, 2504–2526, doi:10.1175/1520-
605   0485(2003)033>2504:NASWTH<2.0.CO:2, 2003.

606 Cooper, L. W., Grebmeier, J. M., Frey, K. E., and Vaglem, S.: Discrete water samples collected
607   from the Conductivity-Temperature-Depth rosette at specific depths, Northern Bering Sea
608   to Chukchi Sea, 2016. Arctic Data Center. doi:10.18739/A23B5W875, 2019.

609 Curry, R., Dickson, R., and Yashayaev, I.: A change in the freshwater balance of the Atlantic
610   Ocean over the past four decades, *Nature*, 426, 826–829, doi:10.1038/nature02206, 2003.

Dombrowsky, E., Bertino, L., Cummings, J., Brassington, G. B., Chassignet, E. P., Davidson, F., Hurlburt, H. E., Kamachi, M., Lee, T., Martin, M. J., Mei, S., and Tonani, M.: GODAE systems in operations. Oceanography, 22(3), 80–95, doi:10.5670/oceanog.2009.68, 2009

Drange, H. and Simonsen, K.: Formulation of air-sea fluxes in the ESOP2 version of MICOM, Technical Report No. 125, Nansen Environmental and Remote Sensing Center, 23 pp., 1996.

Fenty, I., Willis, J. K., Khazendar, A., Dinardo, S., Forsberg, R., Fukumori, I., Holland, D., Jakobsson, M., Moller, D., Morison, J., Meunchow, A., Rignot, E., Schodlock, M., Thompson, A.F., Tino, K., Rutherford, M., and Trenholm, N.: Oceans Melting Greenland: Early results from NASA's ocean-ice mission in Greenland. Oceanography, 29(4):72-83, doi:10.5670/oceanog.2016.100, 2016.

Font, J., Camps, A., Borges, A., Martín-Neira, M., Boutin, J., Reul, N., Kerr, Y. H., Hahne, A., and Mecklenburg, S.: SMOS: The challenging sea surface salinity measurement from space, Proc. IEEE, 98(5), 649–665, doi:10.1109/JPROC.2009.2033096, 2010.

Fournier, S., Lee, T., Wang, X., Armitage, T. W. K., Wang, O., Fukumori, I., and Kwok, R.: Sea Surface Salinity as a Proxy for Arctic Ocean Freshwater Changes. Journal of Geophysical Research: Oceans, 125(7). doi:10.1029/2020JC016110, 2020

Fujii, Y., Rémy, E., Zuo, H., Oke, P., Halliwell, G., Gasparin, F., et al.: Observing system evaluation based on ocean data assimilation and prediction systems: on-going challenges and a future vision for designing and supporting ocean observational networks. *Front. Mar. Sci.,* 6(417), doi:10.3389/fmars.2019.00417, 2019.

Goñi, M. A., Corvi, E. R., Welch, K. A., Buktenica, M., Lebon, K., Alleau, Y., and Juranek, L. W.: Particulate organic matter distributions in surface waters of the Pacific Arctic shelf during the late summer and fall season. Marine Chemistry, 211, 75-93, doi:10.1016/j.marchem.2019.03.010, 2019.

Goñi, M. A., Juranek, L. W., Sipler, R. E., and Welch, K. A.: Particulate organic matter distributions in the water column of the Chukchi Sea during late summer. J. Geophys. Res. Oceans, 126(9), doi:10.1029/2021JC017664, 2021.

Greiner, E., Verbrugge, N., Mulet, S., and Guinehut, S.: Quality information document for multi observation global ocean 3D temperature salinity heights geostrophic currents and MLD product, CMEMS-MOB-QUID-015-012, available at: https://catalogue.marine.copernicus.eu/documents/QUID/CMEMS-MOB-QUID-015-012.pdf (last access: 14 December 2022), 2021.

Janout, M. A., Hölemann, J., Timokhov, L., Gutjahr, O., and Heinemann, G.: Circulation in the northwest Laptev Sea in the eastern Arctic Ocean: Crossroads between Siberian River

646   water, Atlantic water and polynya-formed dense water, J. Geophys. Res. Oceans, 122,
647   6630–6647, doi:10.1002/ 2017JC013159, 2017.

648 Johannessen, O. M., Shalina, E. V., and Miles, M. W.: Satellite evidence for an Arctic Sea ice
649   cover in transformation, *Science*, 286, 1937–1939, doi:10.1126/science.286.5446.1937,
650   1999.

651 Kaminski, T., Kauker, F., Eicken, H., and Karcher, M.: Exploring the utility of quantitative
652   network design in evaluating Arctic sea ice thickness sampling strategies. *The Cryosphere*,
653   9(4), 1721–1733, doi:10.5194/tc-9-1721-2015, 2015

654 Kerr, Y. H., Waldteufel, P., Wigneron, J. P., Delwart, S., Cabot, F., Boutin, J., Escorihuela, M.
655   J., Font, J., Reul, N., Gruhier, C., Juglea, S., Drinkwater, M. R., Hahne, A., Martín-Neira,
656   M., and Mecklenburg, S.: The SMOS mission: New tool for monitoring key elements of the
657   global water cycle, Proc. IEEE, 98(5), 666–687, doi:10.1109/JPROC.2010.2043032, 2010.

658 Lee, T., Lagerloef, G., Gierach, M. M., Kao, H. -Y., Yueh, S. S., and Dohan, K.: Aquarius
659   reveals salinity structure of tropical instability waves. *Geophys. Res. Lett.*, 39, L12610,
660   doi:10.1029/2012GL052232, 2012.

661 Lisæter, K. A., Rosanova, J. and Evensen, G.: Assimilation of ice concentration in a coupled
662   ice-ocean model, using the Ensemble Kalman filter, Ocean Dyn., 53(4), 368–388,
663   doi:10.1007/s10236-003-0049-4, 2003.

664 Lu, Z., Cheng, L., Zhu, J., and Lin, R.: The complementary role of SMOS sea surface salinity
665   observations for estimating global ocean salinity state, J. Geophys. Res. Oceans, 121,
666   doi:10.1002/2015JC011480, 2016.

667 Martin, M. J., King, R. R., While, J., Aguiar, A. B.: Assimilating satellite sea-surface salinity
668   data from SMOS, Aquarius and SMAP into a global ocean forecasting system. Q. J. Roy.
669   Meteor. Soc., 145(719), 705-726, doi:10.1002/qj.3461, 2019.

670 Martínez, J., Gabarró, C., and Turiel, A.: Algorithm Theoretical Basis Document, Arctic+Salinity
671   ITT,   Tech.   rep.,   BEC,   Institut   de   Ciencies   del   Mar-CSIC,
672   doi:10.13140/RG.2.2.12195.58401, 2020.

673 Martínez, J., Gabarró, C., Turiel, A., González-Gambau, V., Umbert, M., Hoareau, N.,
674   González-Haro, C., Olmedo, E., Arias, M., Catany, R., Bertino, L., Raj, R. P., Xie, J., Sabia,
675   R., and Fernández, D.: Improved BEC SMOS Arctic Sea Surface Salinity product v3.1,
676   Earth Syst. Sci. Data, 14, 307–323, doi:10.5194/essd-14-307-2022, 2022.

677 Martín-Neira, M., Oliva, R., Corbella, I., Torres, F., Duffo, N., Durán, I., Kainulainen, J., Closa,
678   J., Zurita, A., Cabot, F., Khazaal, A., Anterrieu, E., Barbosa, J., Lopes, G., Tenerelli, J.,
679   Díez-García, R., Fauste, J., Martín-Porqueras, F., González-Gambau, V., Turiel, A.,
680   Delwart, S., Crapolicchio, R., and Suess, M.: SMOS instrument performance and calibration
681   after six years in orbit. Remote Sens. Environ., 180, doi:10.1016/j.rse.2016.02.036, 2016.

682 Mecklenburg, S., Drusch, M., Kerr, Y. H., Font, J., Martiìn-Neira, M., Delwart, S., Buenadicha,
683   G., Reul, N., Daganzo-Eusebio, E., Oliva, R., and Crapolicchio, R.: ESA's soil moisture and
684   ocean salinity mission: Mission performance and operations, IEEE TGARS, 50, 1354–1366,
685   doi:10.1109/TGRS.2012.2187666, 2012.

686 Olmedo, E., Martínez, J., Turiel, A., Ballabrera-Poy, J., and Portabella, M.: Debiased non-
687   Bayesian retrieval: A novel approach to SMOS Sea Surface Salinity, Remote Sens.
688   Environ., 193, 103–126, doi:10.1016/j.rse.2017.02.023, 2017.

689 Olmedo, E., Gabarró, C., González-Gambau, V., Martínez, J., Ballabrera-Poy, J., Turiel, A.,
690   Portabella, M., Fournier, S., and Lee, T.: Seven Years of SMOS Sea Surface Salinity at
691   High Latitudes: Variability in Arctic and Sub-Arctic Regions. *Remote Sensing*. 2018;
692   10(11):1772, doi:10.3390/rs10111772, 2018.

693 Proshutinsky, A., Krishfield, Timmermans, M.-L., Toole, J., Carmack, E., Mclaughlin, F.,
694   Williams, W. J., Zimmermann, S., Itoh, M., and Shimada, K.: Beaufort Gyre freshwater
695   reservoir: State and variability from observations, J. Geophys. Res. Oceans, 114, 1–25,
696   doi:10.1029/2008JC005104, 2009.

697 Proshutinsky, A., Krishfield, R., and Timmermans, M. -L.: Introduction to special collection on
698   arctic ocean modeling and observational synthesis (FAMOS) 2: beaufort gyre phenomenon.

699   *J. Geophys. Res. Oceans*, 125, e2019JC015400, doi:10.1029/2019JC015400, 2020.

700 Reul, N., Grodsky, S., Arias, M., Boutin, J., Catany, R., Chapron, B., D'Amico, F., Dinnat, E.,
701   Donlon, C., Fore, A., Fournier, S., Guimbard, S., Hasson, A., Kolodziejczyk, N., Lagerloef,
702   G., Lee, T., Le Vine, D., Lindstromn, E., Maes, C., Mecklenburg, S., Meissner, T., Olmedo,
703   E., Sabia, R., Tenerelli, J., Thouvenin- Masson, C., Turiel, A., Vergely, J., Vinogradova, N.,
704   Wentz, F., and Yueh, S.: Sea surface salinity estimates from spaceborne L-band
705   radiometers: An overview of the first decade of observation (2010–2019), *Remote Sens.
706   Environ.,* 242, 111769, doi:10.1016/j.rse.2020.111769, 2020.

707 Rigor, I. G., Wallace, J. M., and Colony, R. L.: Response of Sea Ice to the Arctic Oscillation,
708   *J. Climate*, 15, 2648, doi:10.1175/1520- 0442(2002)015<2648:ROSITT>2.0.CO;2, 2002.

709 Rosenblum, E., Fajber, R., Stroeve, J. C., Gille, S. T., Tremblay, L. B., and Carmack, E. C.:
710   Surface salinity under transitioning ice cover in the Canada Basin: Climate model biases
711   linked to vertical distribution of freshwater. Geophysical Research Letters, 48,
712   e2021GL094739, doi: 10.1029/2021GL094739, 2021

713 Sakov, P., Counillon, F., Bertino, L., Lisæter, K. A., Oke, P. R., and Korablev, A.: TOPAZ4: an
714   ocean-sea ice data assimilation system for the North Atlantic and Arctic, Ocean Sci., 8,
715   633–656, doi:10.5194/os-8-633-2012, 2012.

716 Solomon, A., Heuzé, C., Rabe, B., Bacon, S., Bertino, L., Heimbach, P., Inoue, J., Iovino, D.,
717   Mottram, R., Zhang, X., Aksenov, Y., McAdam, R., Nguyen, A., Raj, R. P., and Tang, H.:
718   Freshwater in the Arctic Ocean 2010–2019, Ocean Sci., 17, 1081–1102, doi:10.5194/os-
719   17-1081-2021, 2021.

720 Steele, M., Morley, R., and Ermold, W.: PHC: A global ocean hydrography with a high-quality
721   Arctic Ocean, J. Climate, 14, 2079–2087, doi: 10.1175/1520-
722   0442(2001)014<2079:PAGOHW>2.0.CO;2, 2001.

723 Storto, A., Alvera-Azcárate, A., Balmaseda, M. A., Barth, A., Chevallier, M., Counillon, F.,
724   Domingues, C. M., Drevillon, M., Drillet, Y., Forget, G., Garric, G., Haines, K., Hernandez,
725   F., Iovino, D., Jackson, L. C., Lellouche, J-M., Masina, S., Mayer, M., Oke, P. R., Penny, S.
726   G., Peterson, K. A., Yang, C. and Zuo, H.: Ocean Reanalyses: Recent Advances and
727   Unsolved Challenges. Front. Mar. Sci., 6(418), doi:10.3389/fmars.2019.00418, 2019.

728 Stroeve, J. and Notz, D.: Changing state of Arctic sea ice across all seasons, Environ. Res.
729   Lett., 13, 103001, https://doi.org/10.1088/1748-9326/aade56, 2018.

730 Stroh, J. N., Panteleev, G., Kirillov, S., Makhotin, M., and Shakhova, N.: Sea-surface
731   temperature and salinity product comparison against external in situ data in the Arctic
732   Ocean. J. Geophys. Res. Oceans, 120, 7223-7236, doi:10.1002/2015JC011005, 2015.

733 Supply, A., Boutin, J., Vergely, J. L., Kolodziejczyk, N., Reverdin, G., Reul, N., and Tarasenko,
734   A.: New insights into SMOS sea surface salinity retrievals in the Arctic Ocean. Remote
735   Sensing of Environment, 249, 112027, doi:10.1016/J.RSE.2020.112027, 2020.

736 Tang, W., Fore, A., Yueh, S., Lee, T., Hayashi, A., Sanchez-Franks, A., Martinez, J., King, B.,
737   and Baranowski, D.: Validating SMAP SSS with in situ measurements, Remote Sens.
738   Environ., 200, 326–340, doi:10.1016/j.rse.2017.08.021, 2017.

739 Tranchant, B., Remy, E., Greiner, E., and Legalloudec, O.: Data assimilation of Soil Moisture
740   and Ocean Salinity (SMOS) observations into the Mercator Ocean operational system:
741   focus on the El Niño 2015 event, Ocean Sci., 15, 543–563, doi:10.5194/os-15-543-2019,
742   2019.

743 Uotila, P., Goosse, H., Haines, K., Chevallier, M., Barthélemy, A., Bricaud, C., Carton, J.,
744   Fu˘ckar, N., Garric, G., Iovino, D., Kauker, F., Korhonen, M., Lien, V. S., Marnela, M.,
745   Massonnet, F., Mignac, D., Peterson, A., Sadikn, R., Shi, L., Tietsche, S., Toyoda, T., Xie,
746   J., and Zhang, Z.: An assessment of ten ocean reanalyses in the polar regions, Clim.
747   Dynam., 52, 1613–1650, doi:10.1007/s00382-018-4242-z, 2019.

748 Vinogradova, N. T., Ponte, R. M., Fukumori, I. and Wang, O.: Estimating satellite salinity errors
749   for assimilation of Aquarius and SMOS data into climate models. J. Geophys. Res. Oceans,
750   119(8), 4732–4744, doi:10.1002/2014JC009906, 2014

751 Woodgate, R. A., Weingartner, T. J., and Lindsay, R.: Observed increases in Bering Strait
752 oceanic fluxes from the Pacific to the Arctic from 2001 to 2011 and their impacts on the
753 Arctic Ocean water column. Geophys. Res. Lett.,39, L24603, doi:10.1029/2012GL054092,
754 2012.

755 Xie, J., Bertino, L., Counillon, F., Lisæter, K. A., and Sakov, P.: Quality assessment of the
756 TOPAZ4 reanalysis in the Arctic over the period 1991-2013. *Ocean Science*, **13**(1). doi:
757 10.5194/os-13-123-2017, 2017.

758 Xie, J., Counillon, F., and Bertino, L.: Impact of assimilating a merged sea-ice thickness from
759 CryoSat-2 and SMOS in the Arctic reanalysis. *The Cryosphere*, **12**(11), 3671-3691. doi:
760 10.5194/tc-12-3671-2018, 2018.

761 Xie, J., Raj, R. P., Bertino, L., Samuelsen, A., and Wakamatsu, T.: Evaluation of Arctic Ocean
762 surface salinities from the Soil Moisture and Ocean Salinity (SMOS) mission against a
763 regional reanalysis and in situ data, Ocean Sci., 15, 1191–1206, doi:10.5194/os-15-1191-
764 2019, 2019.

765 Yu, L.: A global relationship between the ocean water cycle and near-surface salinity, J.
766 Geophys. Res., 116, C10025, doi:10.1029/2010JC006937, 2011.

767 Yu, L., Jin, X., Josey, S. A., Lee, T., Kumar, A., Wen, C., and Xue, Y.: The Global Ocean Water
768 Cycle in Atmospheric Reanalysis, Satellite, and Ocean Salinity, *J. Climate*, *30*(10), 3829-
769 3852, doi:10.1175/JCLI-D-16-0479.1, 2017

770 Yueh, S., West, R., Wilson, W., Li, F., Nghiem, S., and Rahmat- Samii, Y.: Error Sources and
771 Feasibility for Microwave Remote Sensing of Ocean Surface Salinity, IEEE T. Geosci.
772 Remote, 39, 1049–1059, doi: 10.1109/36.921423, 2001.

773 Zweng, M. M., Reagan, J. R., Antonov J. I., Locarnini, R. A., Mishonov, A. V., Boyer, T. P.,
774 Garcia, H. E., Baranova, O. K., Johnson, D. R., Seidov, D., and Biddle, M. M.: World Ocean
775 Atlas 2013, Volume 2: Salinity, Levitus, S. (Ed.), Mishonov, A., Technical Ed. NOAA Atlas
776 NESDIS 74, 39pp, doi:10.7289/V5251G4D, 2013.

Caption and figures:

Table 1. Settings of the three assimilation runs in 2016 with and without SSS.

	Assimilated obs.	Initial model states	End date of assimilation	SSS Observation Errors
Exp0	SST, SLA, T/S profile, SIC, SIT, and SID	6th July	28th Dec.	N/A
ExpV2	SSS V2.0 + obs. used in Exp0	6th July	28th Dec.	Eq. 3
ExpV3	SSS V3.1 + obs. used in Exp0	6th July	28th Dec.	Eq. 3

Table 2. Evaluation of SSS misfits (unit: psu) in the three assimilation runs according to the 6 areas indicated by the blue dashed lines in Fig. 2. The numbers in bold indicate the smallest misfit with a reduction of at least 9% relative to Exp0. The overall score depends on whether the bias and RMSD are reduced by at least 9%. If both criteria are met, the score equals 1, it is 2 if only one of them is met, and 3 otherwise. The star subscript means the bias changes passed the significance test using Student's t-test ($\alpha = 0.05$).

Areas in Fig. 2	Number of obs.	Bias (psu)			RMSD (psu)			Overall score	
		Exp0	ExpV2	ExpV3	Exp0	ExpV2	ExpV3	ExpV2	ExpV3
BS	98	2.81	2.43	***2.08***	2.87	2.54	***2.28***	1*	1*
CS	137	2.32	1.96	***1.91***	2.62	2.26	***2.19***	1*	1*
BSS	189	1.35	1.34	1.30	2.50	2.49	2.47	3	3
NS	669	0.43	0.44	***0.37***	1.19	1.19	1.16	3	2
GS	254	0.50	0.51	***0.24***	1.43	1.43	***1.28***	3	1*
BB	89	0.35	0.37	***0.12***	1.22	1.20	1.22	3	2

24
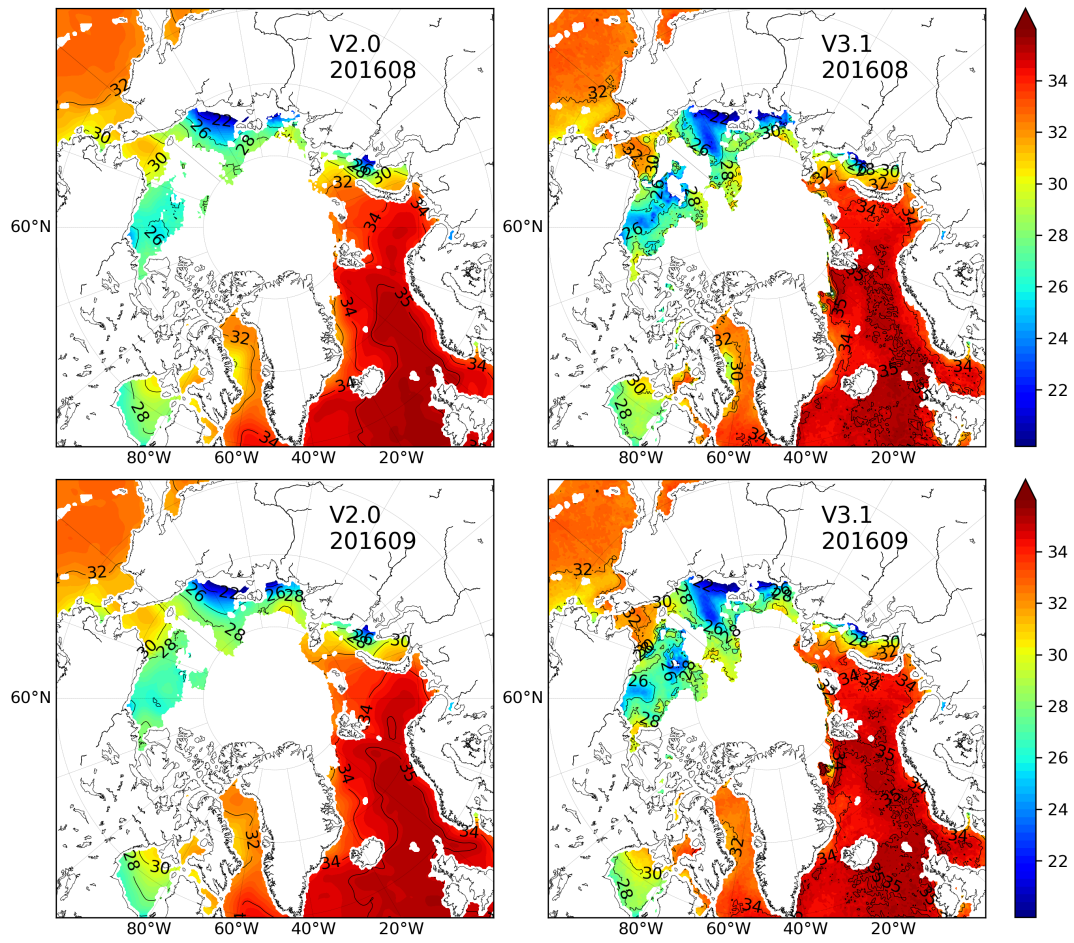
Fig. 1 Monthly SSS of Aug (top line) and Sep (bottom line) in 2016 from SMOS products of BEC V2.0 (left) and V3.1 (right). Note: the solid isolines of SSS are 22, 26, 28, 30, 32, 34, and 35 psu.
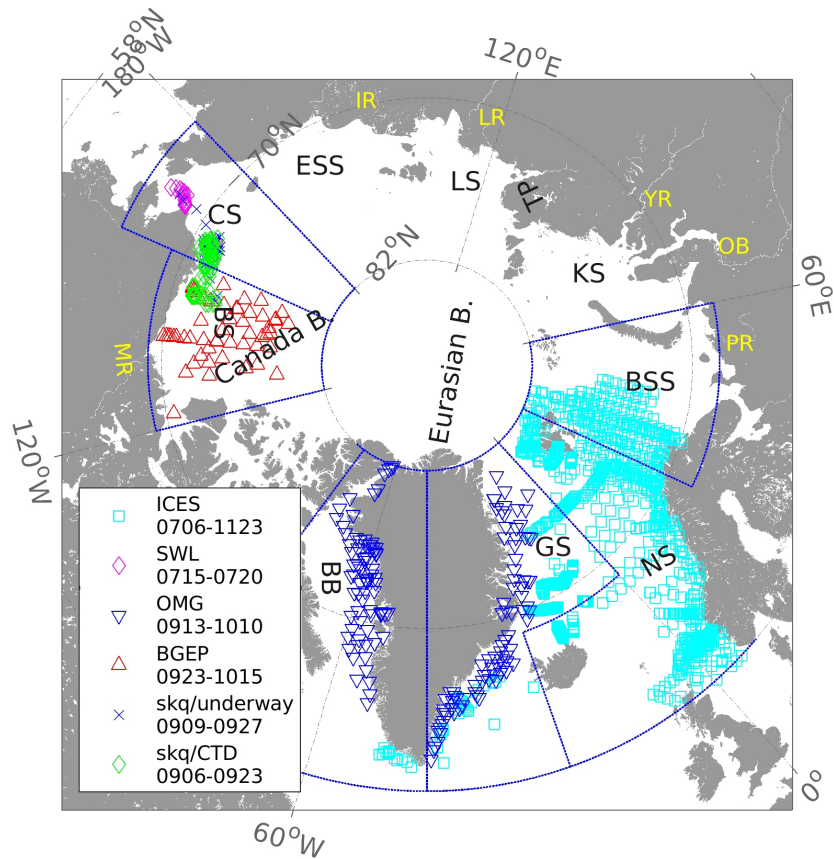
Fig. 2 Locations of the observed SSS from in-situ profiles and surface samples by cruises from July to December 2016. The marks note 6 observation sources, see the details in Section 2.3. The marginal seas delineated are the Beaufort Sea (BS), Chukchi Sea (CS), East Siberian Sea (ESS), Laptev Sea (LS), Kara Sea (KS), Barents Sea (BSS), Greenland Sea (GS), Norwegian Sea (NS), and Baffin Bay (BB). The main rivers around the Arctic region are the Mackenzie River (MR), Pechora (PR), the Ob (OB), Yenisey River (YR), Lena River (LR), and Indigirka River (IR). TP indicates the Taymyr Peninsula.
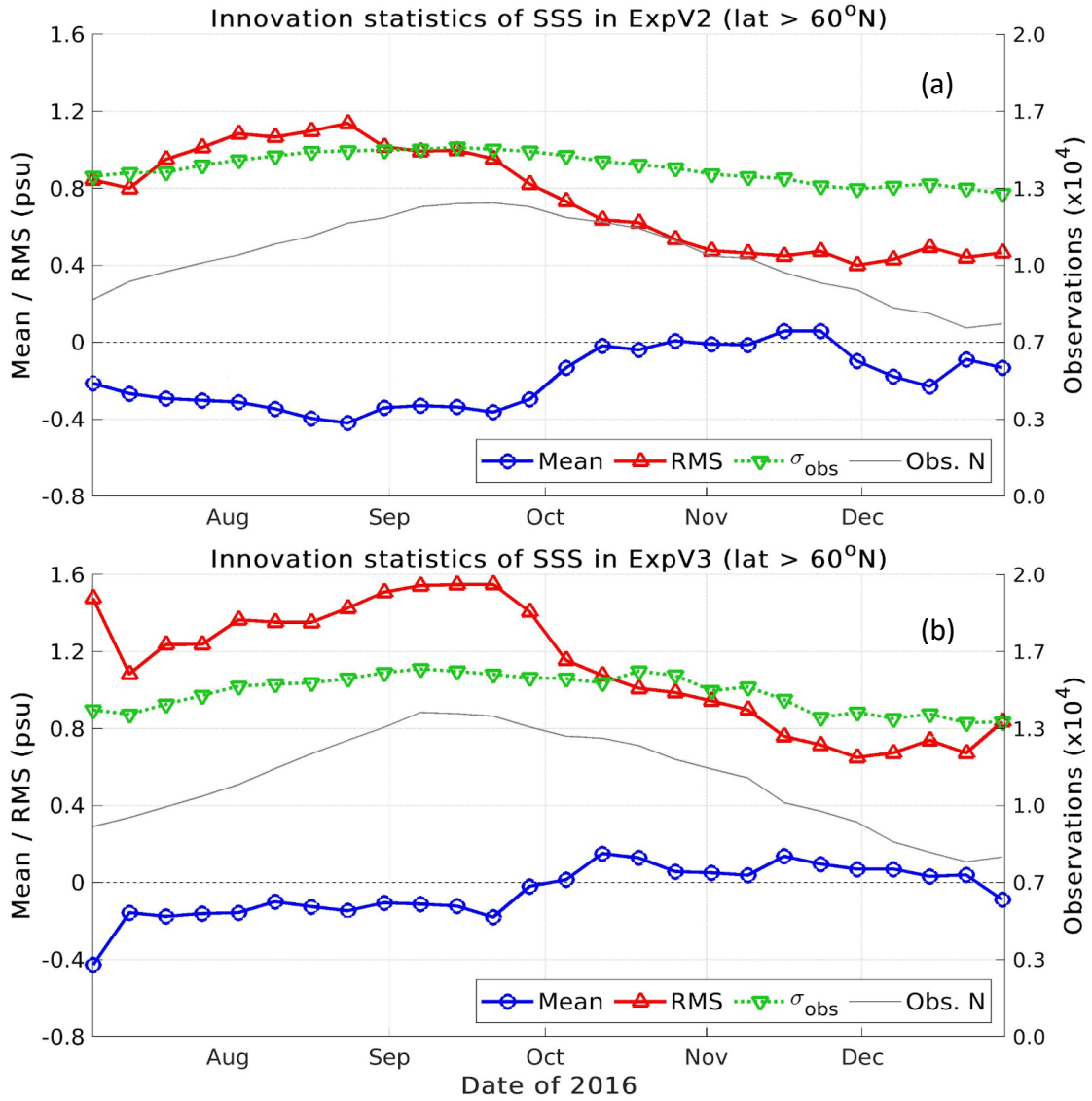
Fig. 3 Innovation statistics of SSS in the Arctic (>60°N) from ExpV2 (a) and ExpV3 (b). The line with red triangles is the root mean squared innovation, and the blue dotted line shows the mean of innovations north of 60°N. The gray line represents the number of observations assimilated, and the green line with inverted triangles is the observation error standard deviation in the two runs.
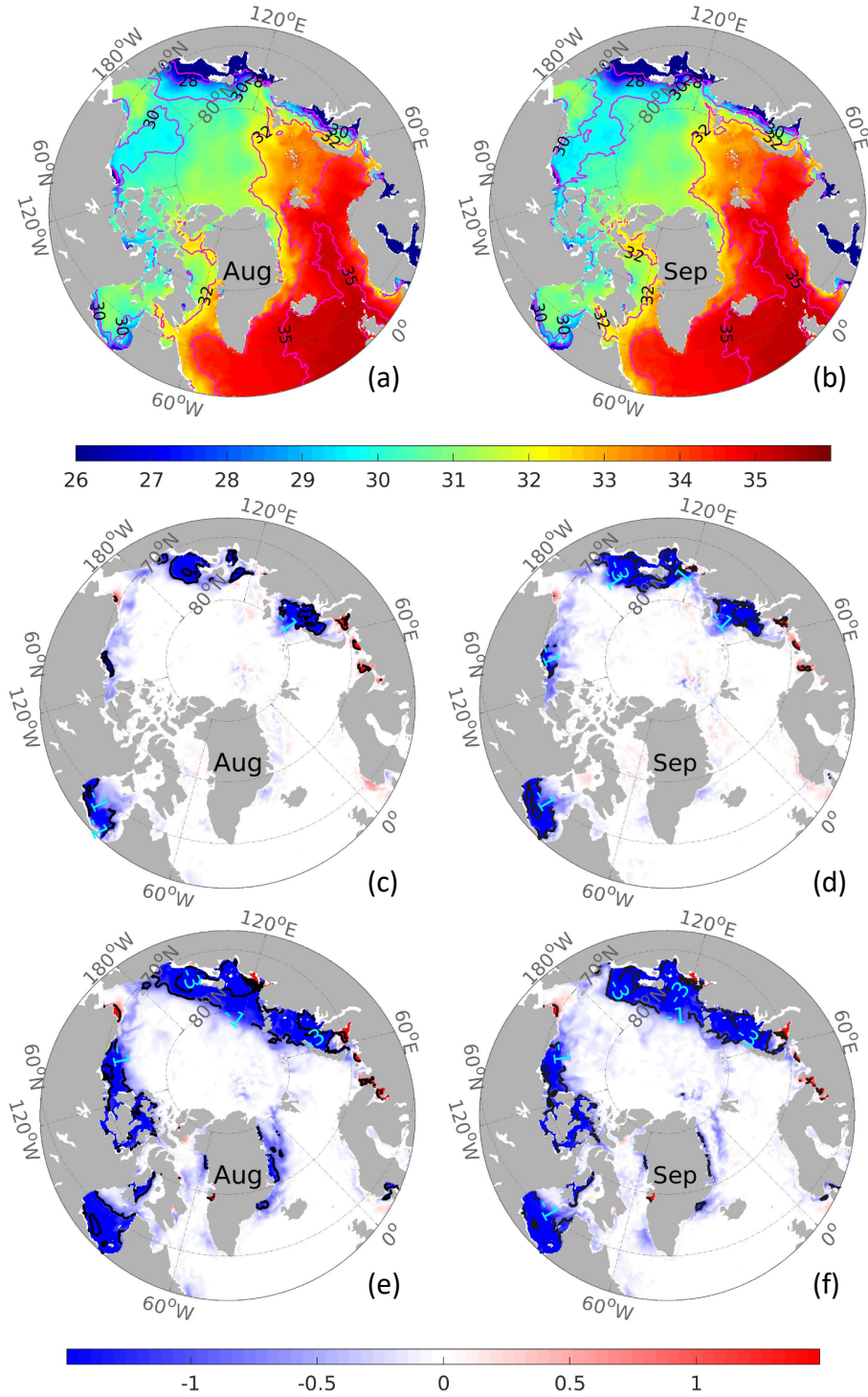
Fig. 4 **Top**: Monthly simulated SSS (unit: psu) from Exp0 in August (left column) and September 2016 (right column). The black isolines indicate the 26, 28, 30, 32, 34, and 35 psu, respectively. **Middle and bottom**: monthly SSS differences in ExpV2 (middle line) and ExpV3 (bottom line) with respect to Exp0. The black lines are -3, -1, 1, and 3 psu.
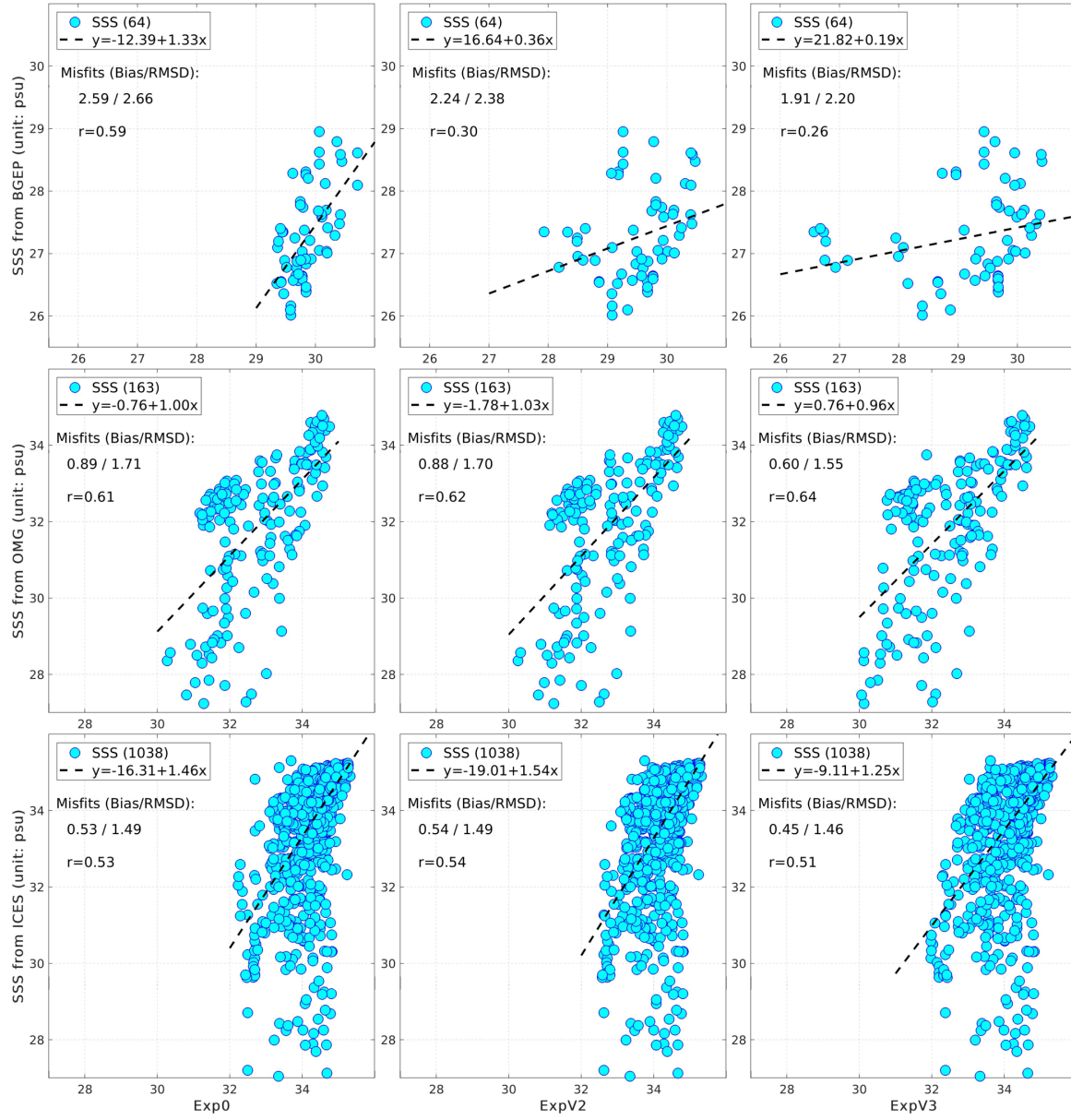
Fig. 5 Scatterplots of SSS in the TOPAZ assimilation runs against in-situ profiles (Top: from BGEP in the Beaufort Sea; Middle: from OMG in both Greenland Seas; Bottom: from ICES in the Nordic Seas as indicated in Fig.1 and descriptions in 2.1). The statistics of SSS misfits are indicated in each panel with the bias and the RMSD, respectively, the number of observations is given between parentheses. The dark dashed line represents the linear regression, and r is the linear correlation coefficient. All the correlation coefficients are over the 95% significance test (α=0.05).
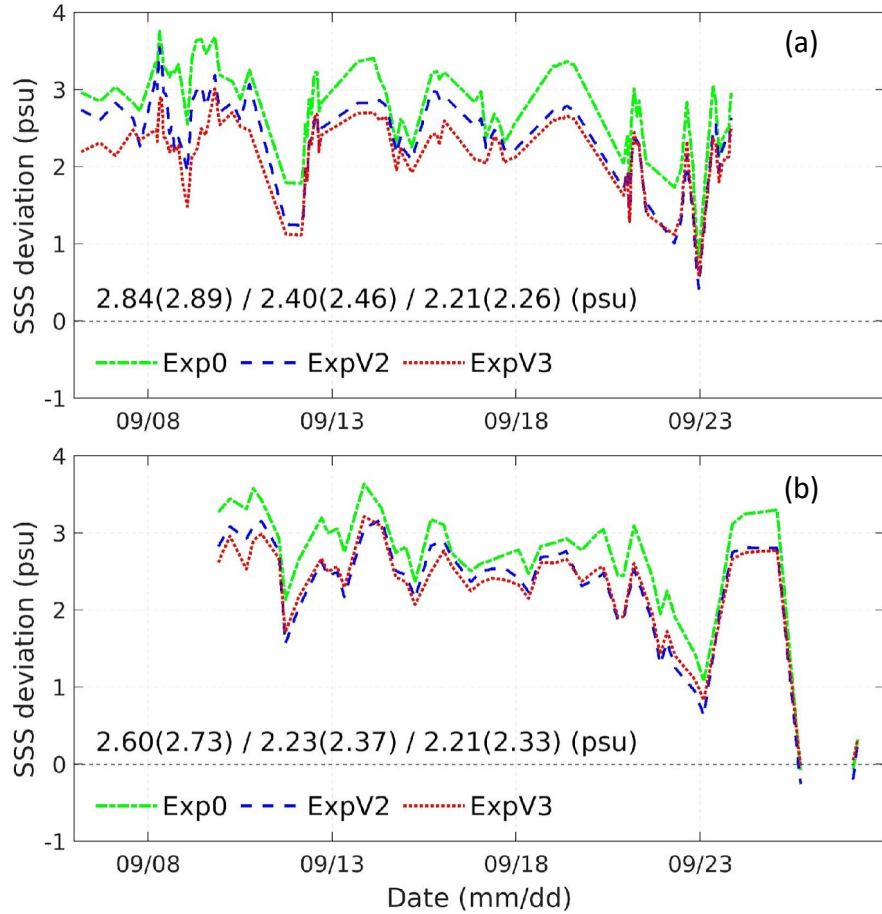
Fig. 6 Model-minus-observations SSS differences in the three assimilation runs against the SSS recorded in the Beaufort Sea and the Chukchi Sea along the SKQ cruise in 2016: a) from CTD profiles; b) from surface water samples underway in the same cruise. The biases are indicated in the same order and the corresponding RMSD are between parentheses.
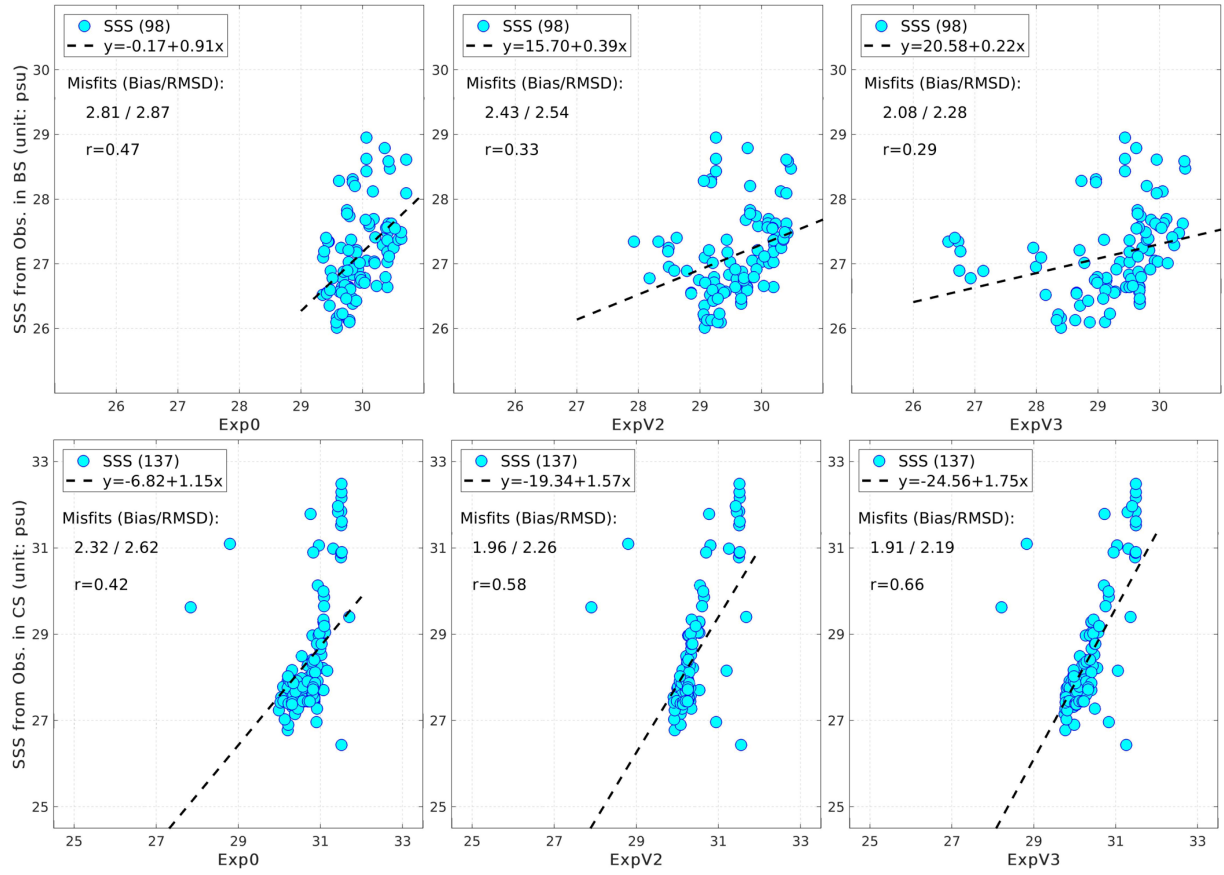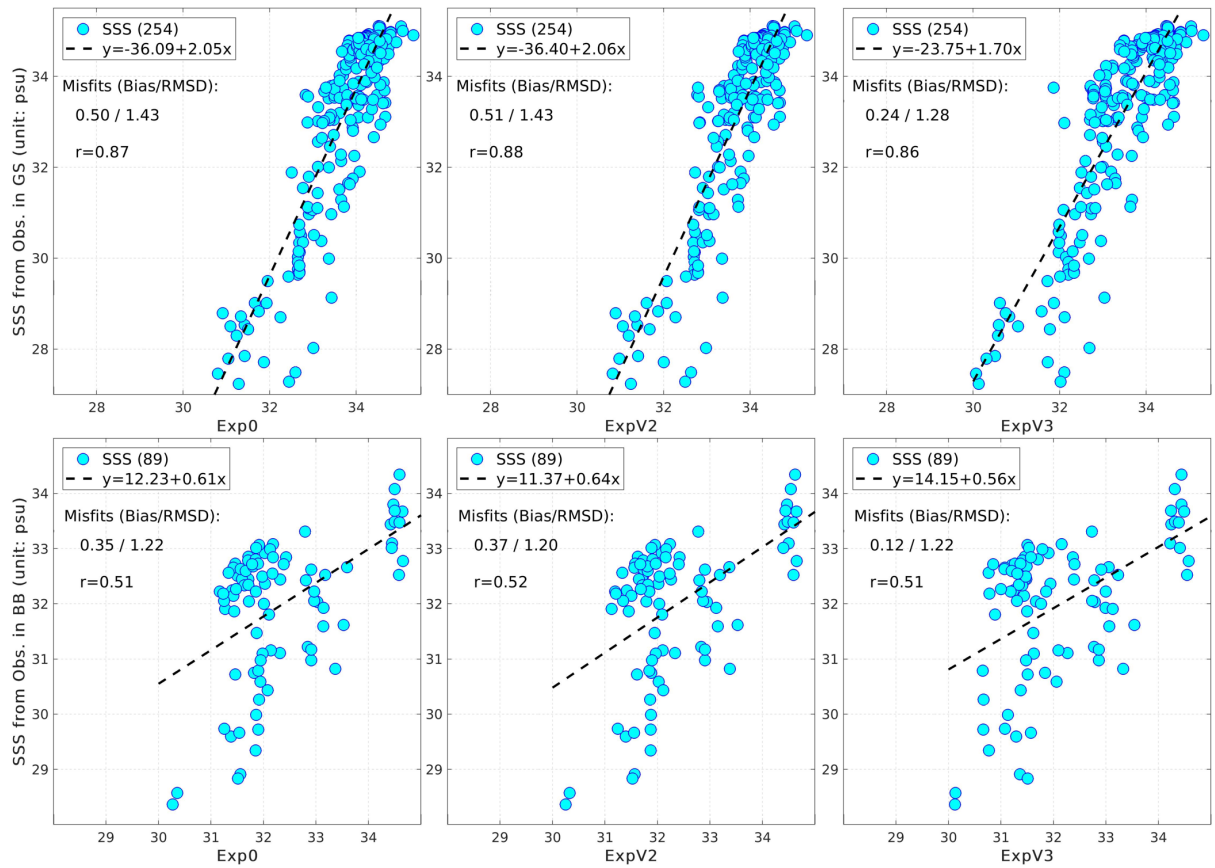
Fig. 7 Scatterplots of SSS (unit: psu) in the three assimilation runs Exp0, ExpV2, and ExpV3 against the CTD observations collected by different cruises in 2016. **Top**: Beaufort Sea; **Bottom**: Chukchi Sea as shown in Fig.1. All the correlation coefficients are over the 95% significance test (α=0.01).

Fig. 8 Scatterplots of SSS (unit: psu) in the three assimilation runs Exp0, ExpV2, and ExpV3 against CTD observations from OMG and ICES in 2016. **Upper**: East Greenland Sea; **Bottom**: Baffin Bay as shown in Fig.1. The statistics of SSS misfits are indicated in each panel with the bias and the RMSD respectively, and the number of observations is given between parentheses. The dark dashed line represents the linear regression, and r is the linear correlation coefficient. All the correlation coefficients are over the 95% significance test (α=0.01).
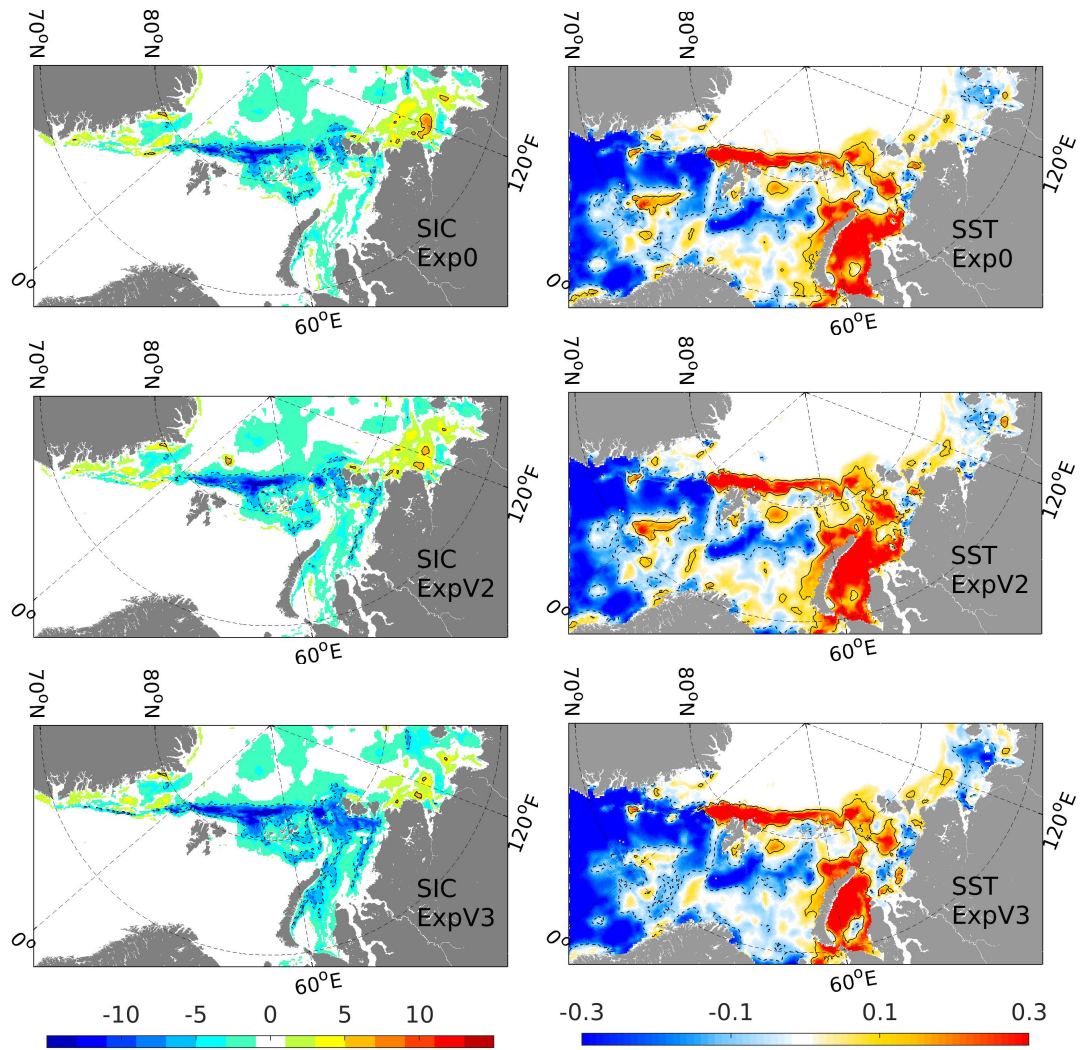
Fig 9. Averaged increments for the 6-months period (Top: in Exp0; Middle: in ExpV2; Bottom: in ExpV3). The figure shows the European Arctic for clarity. Left column: sea ice concentration (unit: %) with isolines of ± 5%. Right column: SST with isolines of ± 0.1°C.
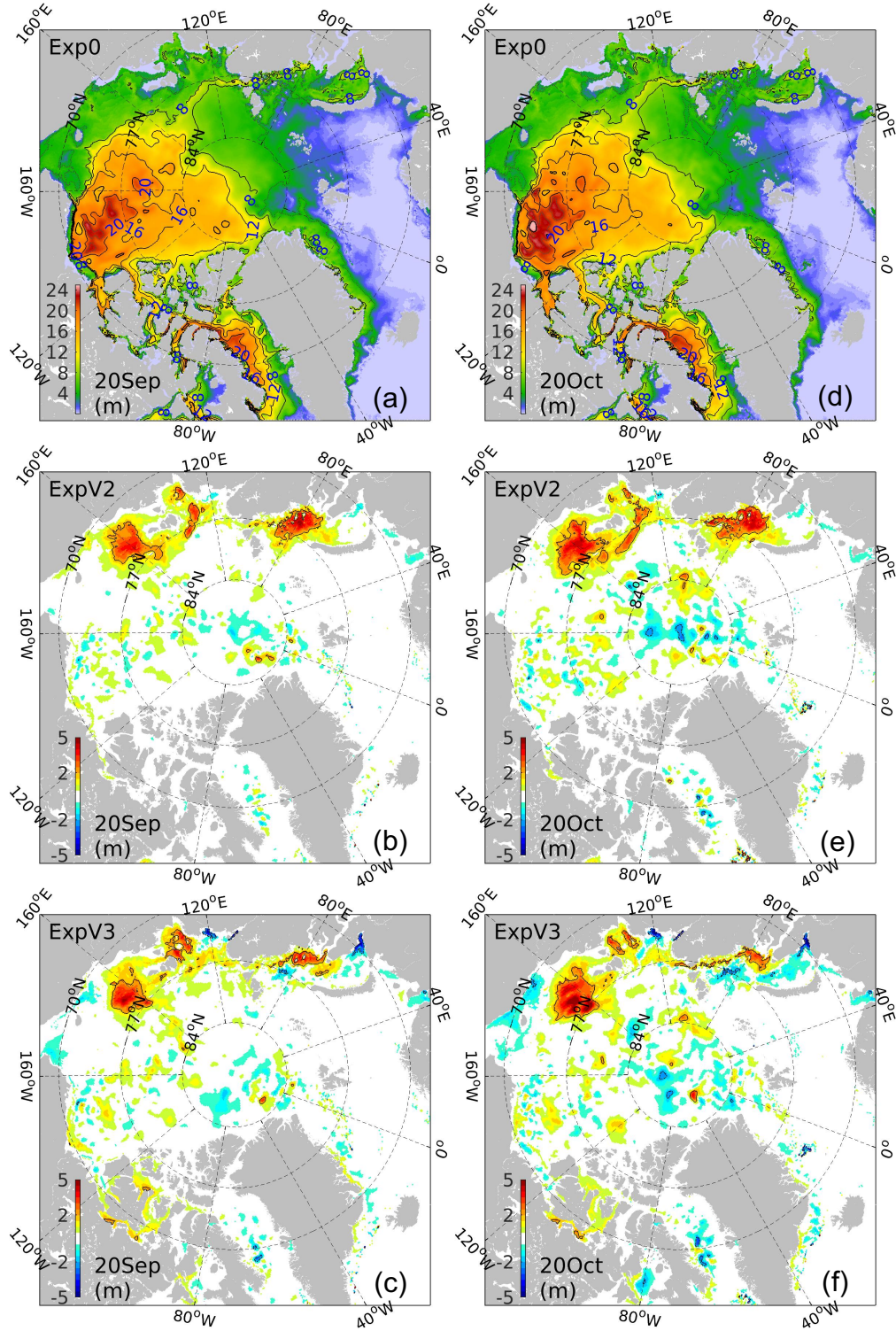
Fig. 10 Top: Freshwater contents (unit: m) on 20th September and 20th October 2016 in the Arctic Ocean from the three assimilation runs: Exp0. The interval of isolines is 4 meters. **Middle and bottom**: the FWC differences in ExpV2 (middle line) and ExpV3 (bottom line) concerning that in Exp0. The black lines indicate -2 m and 2 m differences.
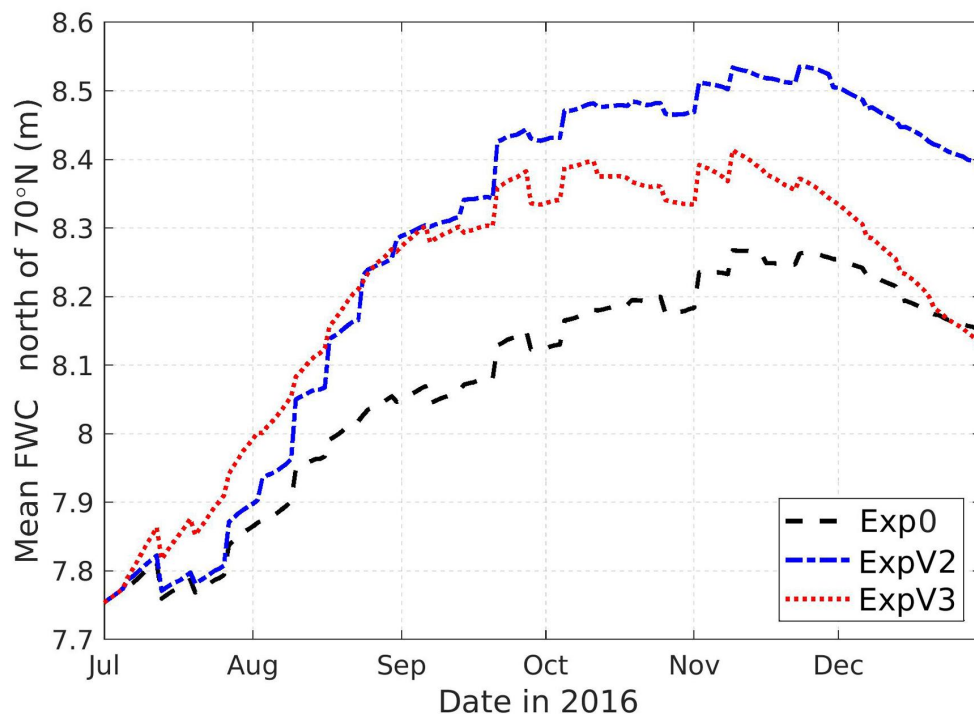
Fig 11. Arctic-wide averaged freshwater content (unit: m) in the central Arctic (>70°N) from July to December 2016 for Exp0 (dark dashed), ExpV2 (blue dashed), and ExpV3 (red dotted).